ACS BIO & MED CHEM Au
AN OPEN ACCESS JOURNAL OF THE AMERICAN CHEMICAL SOCIETY

pubs.acs.org/biomedchemau

Article

Synergetic Antimicrobial Activity and Mechanism of Clotrimazole-Linked CO-Releasing Molecules

Sofia S. Mendes, Joana Marques, Edit Mesterházy, Jan Straetener, Melina Arts, Teresa Pissarro, Jorgina Reginold, Anne Berscheid, Jan Bornikoel, Robert M. Kluj, Christoph Mayer, Filipp Oesterhelt, Sofia Friães, Beatriz Royo, Tanja Schneider, Heike Brötz-Oesterhelt,* Carlos C. Romão,* and Lígia M. Saraiva*

Cite This: *ACS Bio Med Chem Au* 2022, 2, 419–436

Read Online

ACCESS | Metrics & More | Article Recommendations | Supporting Information

ABSTRACT: Several metal-based carbon monoxide-releasing molecules (CORMs) are active CO donors with established antibacterial activity. Among them, CORM conjugates with azole antibiotics of type $[Mn(CO)_3(2,2'\text{-bipyridyl})(azole)]^+$ display important synergies against several microbes. We carried out a structure−activity relationship study based upon the lead structure of $[Mn(CO)_3(Bpy)(Ctz)]^+$ by producing clotrimazole (Ctz) conjugates with varying metal and ligands. We concluded that the nature of the bidentate ligand strongly influences the bactericidal activity, with the substitution of bipyridyl by small bicyclic ligands leading to highly active clotrimazole conjugates. On the contrary, the metal did not influence the activity. We found that conjugate $[Re(CO)_3(Bpy)(Ctz)]^+$ is more than the sum of its parts: while precursor $[Re(CO)_3(Bpy)Br]$ has no antibacterial activity and clotrimazole shows only moderate minimal inhibitory concentrations, the potency of $[Re(CO)_3(Bpy)(Ctz)]^+$ is one order of magnitude higher than that of clotrimazole, and the spectrum of bacterial target species includes Gram-positive and Gram-negative bacteria. The addition of $[Re(CO)_3(Bpy)(Ctz)]^+$ to *Staphylococcus aureus* causes a general impact on the membrane topology, has inhibitory effects on peptidoglycan biosynthesis, and affects energy functions. The mechanism of action of this kind of CORM conjugates involves a sequence of events initiated by membrane insertion, followed by membrane disorganization, inhibition of peptidoglycan synthesis, CO release, and break down of the membrane potential. These results suggest that conjugation of CORMs to known antibiotics may produce useful structures with synergistic effects that increase the conjugate's activity relative to that of the antibiotic alone.

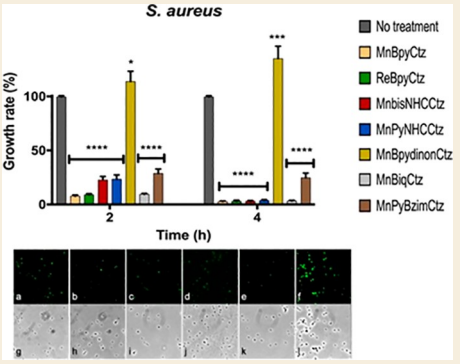

KEYWORDS: *carbon monoxide-releasing molecules, carbon monoxide, antimicrobials, membrane depolarization, peptidoglycan synthesis inhibition, lipid II, Staphylococcus aureus*

In the wake of the rapidly expanding studies on carbon monoxide (CO) biology and therapy, which revealed a broad area of applications,[1] some of us decided to investigate the influence of CO on bacteria. For this purpose, we used gaseous CO and several metal-based CO-releasing molecules (CORMs) that had been established as therapeutically active CO donors in *in vivo* disease models. We found that several of those CORMs had significant antibacterial activity toward both Gram-positive and Gram-negative bacteria, whereas others were weaker or even innocuous.[2] The readily available and most widely used Ru(II)-based CORM-2 and CORM-3 (Figure 1) were among the more potent CORMs in this seminal study, and thus, they were selected for further studies by us and others. Much attention was devoted to the understanding of the mode of action (MoA) of this new class of antimicrobials. Despite serious efforts, the MoA still is not completely understood, and a full account of its details has been given.[3,4] There are data clearly supporting the action of CO and data favoring the dominant action of Ru(II) ions, as well as data countering each of these possibilities. This is due to the very labile nature of both CORM-2 and CORM-3 in biological media and their unusual and very complex chemistry.[5,6] In any case, the potential utility of these CORMs, and certainly of other new antimicrobials overcoming bacterial resistance, became evident in three studies showing that CORM-3 offers protection to rodents infected with *Pseudomonas aeruginosa*;[7] CORM-2 potentiates the effect of antibiotics, for example, by resensitizing a metronidazole-resistant *Helicobacter pylori* strain;[8] and CORM-2, in

Received: January 27, 2022
Revised: March 24, 2022
Accepted: March 24, 2022
Published: April 8, 2022

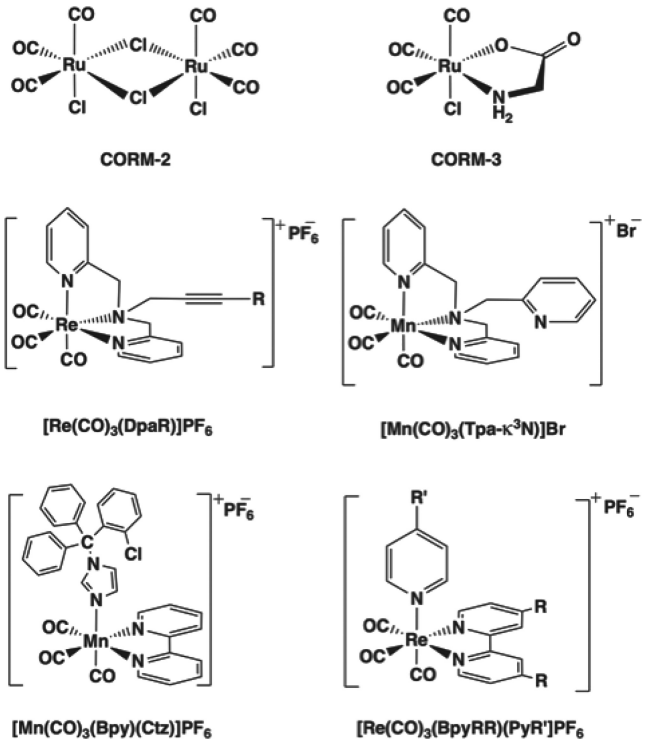

Figure 1. Selected CORMs with antimicrobial activity.

combination, increases the efficiency of tobramycin against *P. aeruginosa*.[9]

In order to better evaluate the role of CO as a bactericidal agent, Schatzschneider and co-workers introduced the structurally stable CORM $[Mn(CO)_3(Tpa\text{-}\kappa^3N)]Br$ (Figure 1) and studied its bactericidal action on *Escherichia coli*. The compound requires photoactivation to release CO. The proposed overall mechanism is complex and includes the destruction of the bacterial membrane by $HO^{\bullet}$ radicals formed in the reaction of the partially CO-depleted fragment $[Mn(CO)_2(Tpa\text{-}\kappa^3N)]^+$ with H_2O_2 generated in the cytoplasm.[10,11] In agreement with the results obtained with CORM-2 and CORM-3, this photoCORM synergized with doxycycline and colistin to better kill a multidrug resistant avian pathogenic *E. coli* strain.[10,12]

Also moving to more structurally stable metal carbonyl compounds, Metzler-Nolte and co-workers studied a family of complexes of the general formula $[Re(CO)_3(DpaR)]^+$, where R represents a series of substituents on the central amine of the tripodal di-(2-picolyl)amine (Dpa) ligand (Figure 1). Several of these complexes displayed high activity against Gram-positive bacteria, but activity against Gram-negative bacteria was not detected.[13,14] In an elegant structure−activity relationship (SAR) study, they established that high activity (minimal inhibitory concentration, MIC ≈ 2−4 μg/mL) was only met for certain types of R chains, based upon peptide nucleic acids (PNAs), and that the $[Re(CO)_3]^+$ metal fragment was necessary but not a sufficient condition to impart bactericidal activity to the (DpaR) ligand structure. The MoA study indicated that the compound affects the membrane potential and membrane integrity, as well as cell wall integrity, thereby inducing cell membrane blebbing. Similar compounds were shown to have bactericidal activity in the dark and more strongly under light irradiation, killing both Gram-positive and Gram-negative bacteria.[15]

In a slightly different approach, Schatzschneider and co-workers reported that the conjugated CORMs $[Mn(CO)_3(Bpy)(azole)][PF_6]$ (where the azole was miconazole, ketoconazole, or clotrimazole (Ctz)) had much higher activity against a panel of Gram-positive bacteria and parasites than the azole alone. In particular, the $[Mn(CO)_3(Bpy)(Ctz)][PF_6]$ derivative (Figure 1) showed the highest activity (up to 30-fold higher than that of Ctz alone) against the eukaryotic parasites *Leishmania major* and *Trypanosoma brucei*.[16] Interestingly, the lowest MIC values of 0.6 μM are close to those reported for the active $[Re(CO)_3(DpaR)]^+$ molecules, and no mention of any CO participation in the mechanism is made in both studies. More recently, phosphopyricin, a phosphine derivative of the $W(CO)_5$ fragment, $W(CO)_5\{PPh_2(C3\text{-pyrrole})\}$, has also shown activity in the same MIC range, with the property of losing activity upon exposure to light.[17]

Metzler-Nolte and co-workers also reported potent bactericides against Gram-positive bacteria based on the $[Re(CO)_3(BpyRR)X]^{0,1+}$ scaffold where BpyRR represents substituted bipyridyl and X represents N-heterocyclic carbene (NHC) ligands derived from benzimidazole.[18] Along these lines, Zobi and collaborators have demonstrated the enormous antimicrobial potential of $[Re(CO)_3(L{-}L)X]^{0,1+}$ complexes in two outstanding screening studies published while this work was ongoing.[19,20] A number of highly potent derivatives of the $[Re(CO)_3(BpyRR)X]^{0,1+}$ framework (X = pyridine-based ligands) were found to be active against *Staphylococcus aureus*, methicillin-resistant *Staphylococcus aureus* (MRSA), and *Candida albicans* in the sub-micromolar or low micromolar range. Importantly, these molecules (Figure 1) were devoid of important toxicity, presented high therapeutic indexes, and even outperformed linezolid and vancomycin.[19,20]

It is now clear that the $[M(CO)_3]$ fragment, which is present in all of these complexes as well as in $W(CO)_5\{PPh_2(C3\text{-pyrrole})$, enables the assembly of a range of metal carbonyl complexes with potent bactericidal activity. However, the true mechanistic MoA of these complexes has not been studied in detail, and it may differ among the different types of scaffolds.

The $[Mn(CO)_3(Bpy)(azole)]^+$ conjugates are very interesting species since different types displayed important synergies with other antibiotics, to the point of reverting acquired antibiotic resistance features in some bacteria. In this work, we sought to better understand the MoA of these CORM conjugates as well as modulate and improve their activity as antimicrobials. For this purpose, a SAR study based upon the $[Mn(CO)_3(Bpy)(Ctz)]^+$ lead structure was carried out, producing several conjugates with varying metals and ligands, which were tested for their antimicrobial activity and MoA.

RESULTS

Design, Synthesis, and Characterization of CORM−Clotrimazole Conjugates

Considering that the $[M(CO)_3]$ fragment is a potential determinant of the antibacterial activity,[16] we used the structure of $[Mn(CO)_3(Bpy)(Ctz)][PF_6]$ (Bpy = 2,2′-bipyrydine and Ctz = clotrimazole) as the lead to this SAR study intended to gain mechanistic insights into the MoA of these type of metal carbonyl complexes. For this purpose, several analogues of $[Mn(CO)_3(Bpy)(Ctz]PF_6]$ were synthesized with the following modifications: (i) replacement of Mn with Re; (ii) introduction of a chemical substitution on the Bpy ligand; (iii) replacement of bipyridine ligands with other

https://doi.org/10.1021/acsbiomedchemau.2c00007
ACS Bio Med Chem Au 2022, 2, 419−436

Scheme 1. Synthesis of the Clotrimazole−CORM Conjugates[a]

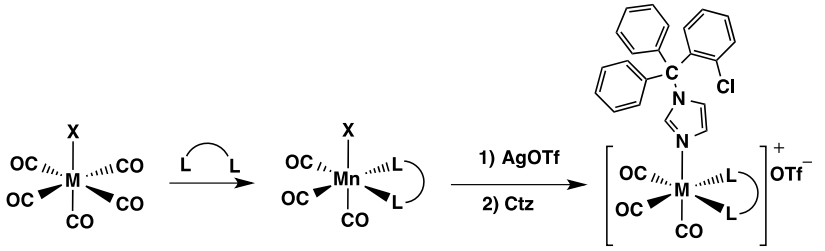

[a]M = Mn and Re; X = Br and I; OTf = O_3SCF_3 (triflate); L−L = Bpy, Biq, PyBzim, Bpydinon, PyNHC, and bisNHC; and Ctz = clotrimazole. OTf (O_3SCF_3, triflate).

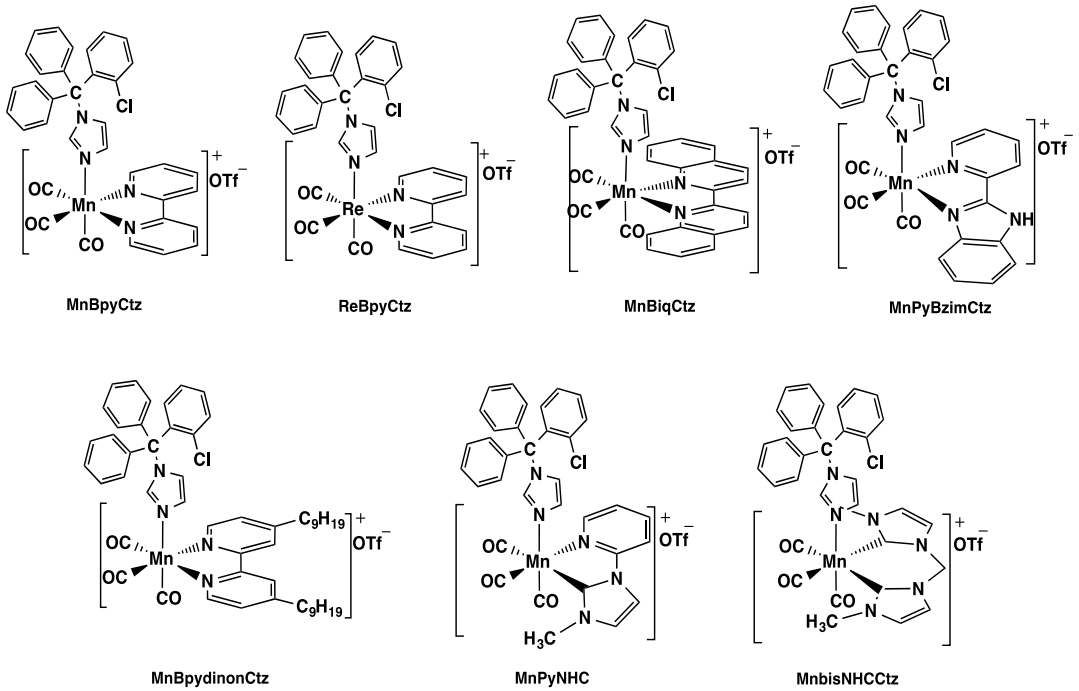

Figure 2. Conjugates prepared by combining the *fac*-{$M(CO)_3$}d^6 fragment with bidentate ligands and clotrimazole.

diimine ligands; and (iv) introduction of nondiimine bidentate ligands with different electronic and steric requirements.

We started from $Mn(CO)_5Br$ (aka ALF021[2]), and the conjugates were prepared, along with a series of useful intermediates using the stepwise approach depicted in Scheme 1. In this way, several isostructural and isoelectronic conjugate complexes were prepared (Figure 2). Since all these compounds have a common set of four ligands (3xCO + Ctz) as well as the same counterion, triflate, we will identify them by the symbols of the metal and the bidentate ligand, thus facilitating their identification when comparing properties, for example, $[Mn(CO)_3(Bpy)(Ctz)]OTf$ = **MnBpyCtz** and $[Mn(CO)_3(Bpy)Br]$ = **MnBpyBr**.

These clotrimazole conjugates are all 18-electron monocationic species. As solids, they are stable against laboratory manipulation in air and under ordinary light for short periods. They are routinely kept in the dark under nitrogen and, when necessary, are dissolved in deoxygenated solvents except for the biologic tests. The synthetic procedures are described in the Materials and Methods section along with the spectroscopic data. All compounds were characterized using elemental analysis, Fourier transform infrared (FTIR) spectroscopy, ^{1}H NMR, and, when necessary, by ^{13}C NMR and high-resolution mass spectrometry (HRMS). FTIR data on νCO stretching vibrations (Supporting Information Table S1) confirm the presence of facial *fac*-{$M(CO)_3$}d^6 fragments in all the prepared complexes.

Compound $[Mn(CO)_3(Bpy)(Ctz)][OTf]$ (**MnBpyCtz**) (Figure 2) was prepared as previously described.[16] The rhenium analogue **ReBpyCtz** was synthesized from the known *fac*-$[Re(CO)_3(Bpy)Br]$ (**ReBpyBr**). The ν_{sym}CO stretching vibration (Supporting Information Table S1) is slightly lower for **ReBpyCtz** (2029 cm^{-1}) than for **MnBpyCtz** (2038 cm^{-1}), which is the complex with the highest ν_{sym}CO value of all the complexes shown in Figure 2 ,indicating the more efficient π-acceptance of this ligand in this set of compounds. The 2,2′-biquinoline (Biq) complex, **MnBiqCtz**, derived from well-characterized *fac*-$[Mn(CO)_3(Biq)Br]$,[21] extends the ligand bulk on the equatorial plane as well as the π cloud of the bidentate ligand. The latter extension is reflected in the red color of **MnBiqCtz**, which contrasts with the yellow or yellowish color of all the other complexes. The values of the ν_{sym}CO stretching vibrations are intermediate between those of **ReBpyCtz** and **MnBpyCtz**. Conjugate **MnPyBzimCtz** extends the bulk of the N−N bidentate ligand also on the equatorial plane of the complex but in an asymmetric manner. Its ν_{sym}CO

https://doi.org/10.1021/acsbiomedchemau.2c00007
ACS Bio Med Chem Au 2022, 2, 419−436

stretching vibration is clearly lower (*ca.* 14 cm^{-1}) than that of **MnBpyCtz**, in agreement with a lower π-acceptance of the pyridine-benzimidazole ligand relative to the Bpy ligand. Complex **MnBpydinonCtz** contains a Bpy ligand modified by the presence of two C9-alkyl chains in positions 4 and 4′ of the heterocyclic rings. Such chains impart a marked stereochemical bulk on the distal side of the $[Mn(CO)_3]$ face. This substitution produces a *ca.* 10 cm^{-1} decrease in the $\nu_{sym}CO$ stretching vibration when compared to **MnBpyCtz**, which agrees with a reinforced π-back donation due to the electron donating effect of the alkyl substituents that increase the electron density at the metal.

A new subset of complexes with other small, bidentate ligands was also assembled. In this smaller set, the ligands have higher σ-donating and lower π-accepting ability. In particular, we used imidazolium-derived NHC ligands, which are very strong carbon σ-donors that have been extensively used in catalysis. The bidentate ligand in **MnPyNHCCtz** features one N-bound pyridine ring and one C-bound NHC. From the structural point of view, this ligand is flat, making the fragment $[Mn(CO)_3(PyNHC^{Me})]^+$ very compact, similar to the Bpy analogue. The $\nu_{sym}CO$ for **MnPyNHCCtz** is similar to that in **MnBiqCtz** and **MnBpydinonCtz**, indicating a fairly efficient π-acceptance. The $bisNHC^{Me}$ ligand featured in **MnbisNHCCtz** is an even more powerful electron donor to the $[Mn(CO)_3(Ctz)]^+$ fragment, and this is reflected in the lowest $\nu_{sym}CO$ stretching vibration (2013 cm^{-1}) of all shown conjugates. However, in contrast to the $PyNHC^{Me}$ ligand, the $BisNHC^{Me}$ ligand is not flat with both methyl substituents on the N2C3 rings pointing to the same side of the equatorial plane.[22] Therefore, complex **MnbisNHCCtz** is the first in this series without a flat equatorial ligand. Nevertheless, the stability imparted by the $BisNHC^{Me}$ ligand in **MnbisNHCCtz** is very high, judging by its air stability and the robust catalytic activity of its precursor $[Mn(CO)_3(BisNHC^{Me})Br]$ in the catalytic reduction of CO_2 to CO.[22]

Taken together, this small library of complexes contains species that have the same type of geometrical structure (octahedral around the metal with the same relative arrangement of the three CO and Ctz ligands), the same positive charge (1^+), the same counterion (triflate), a continuum of electron density at the metal (thus reactivity), as judged by the range of νCO values, and a few small structural variations concerning the bulk of the equatorial plane containing the bidentate ligand and two CO ligands. Below, we show how these small differences influence the antibacterial activity of the CORM complexes.

Bactericidal Properties of CORM−Clotrimazole Conjugates

We first used three model bacterial pathogens to characterize the antimicrobial activity of the synthesized CORMs, namely, two Gram-negative species *E. coli* and *Salmonella enterica*, and Gram-positive MRSA. Several compounds among our set of CORM−Ctz conjugates demonstrated single-digit micrograms per milliliter MIC values against *S. aureus*, and, notably, several of them outperformed free clotrimazole (Table 1). **ReBpyCtz** was 4 times more active than its Mn analogue **MnBpyCtz**, while both of their clotrimazole-depleted precursors, namely, **ReBpyBr** and **MnBpyBr**, respectively, did not show antibacterial activity against these bacteria up to 32 μg/mL (Table 1). Cultures of *E. coli* and *S. enterica* still showed residual turbidity after overnight incubation with CORMs (Table 1), and most compounds were not active enough to inhibit growth sufficiently for an MIC readout. Nonetheless, several compounds reduced the growth rate also for the Gram-negative species (Supporting Information Table S2).

Table 1. MICs of Conjugate CORMs (A) and of ReBpyCtz and Its Synthetic Precursors (B) against the Indicated Bacteria[a]

A	*S. aureus*	*E. coli* K12	*S. enterica*
MnBpyCtz	2	>32	>32
ReBpyCtz	0.5	>32	>32
MnBiqCtz	8	>32	>32
MnPyBzimCtz	10	>32	>32
MnBpydinonCtz	>32	>32	>32
MnPyNHCCtz	0.5	>4	Nd[b]
MnbisNHCCtz	0.5	>4	Nd[b]
MnBpyBr	>32	>32	>32
ReBpyBr	>32	>32	>32
MnPyNHCI	>4	>4	Nd[b]
MnbisNHCBr	>4	>4	Nd[b]
Ctz	4	>32	>32

B	Ctz	**ReBpyBr**	**ReBpyCtz**
B. subtilis 168	2	>32	0.25
S. aureus ATCC29213	8	>32	0.25
S. aureus NCTC8325	4	>32	0.25
S. aureus MRSA	4	>32	0.5
E. faecium BM4147-1	8	>32	2
E. coli ATCC25922	>32	>32	16
K. pneumoniae ATCC12657	>32	>32	32
E. aerogenes ATCC13048	>32	>32	32
P. aeruginosa ATCC27853	>32	>32	32
A. baumannii 09987	>32	>32	8

[a]MICs (μg/mL) were determined as described in the Materials and Methods section and for at least three biological samples. [b]Nd—not determined.

To further discriminate the conjugate CORMs' activity, we evaluated the growth of *S. aureus*, *E. coli*, and *S. enterica* when treated with CORMs (Figure 3 and Supporting Information Table S2).

Several CORM−Ctz conjugates reduced the growth of Gram-negative bacteria, with **ReBpyCtz** showing the highest activity against *E. coli* (a reduction of ∼63% of growth after 4 h) and *S. enterica* (a reduction of ∼37% growth after 4 h). For *E. coli* and *S. enterica*, a reproducible impact on growth was observed only for CORMs with the smaller ancillary rings, namely, **MnBpyCtz**, **ReBpyCtz**, **MnPyNHCCtz**, and **MnbisNHCCtz**. While cells exposed to **MnBpyCtz** after 4 h recovered and exhibited a growth behavior similar to that of nonexposed cells (93% growth relative to untreated cells), no growth recovery occurred for *E. coli* or *S. enterica* exposed to **ReBpyCtz**.

All CORM−Ctz conjugates were toxic to *S. aureus*, except **MnBpydinonCtz**, causing a significant growth decrease in the following order: **MnPyBzimCtz** < **MnbisNHCCtz** ≈ **MnPyNHCCtz** < **MnBiqCtz** ≈ **MnBpyCtz** ≈ **ReBpyCtz** (Supporting Information Table S2). Prolonged exposure of *S. aureus* (∼4 h) to the latter five conjugates reduced growth to values of only 2−4% of those of untreated cells (Supporting Information Table S2).

Altogether, these results revealed a set of new CORMs with antimicrobial properties that go beyond the effect of free clotrimazole. All complexes have a common structural fragment $[M(CO)_3(Ctz)]^+$, which is bound to several different

https://doi.org/10.1021/acsbiomedchemau.2c00007
ACS Bio Med Chem Au 2022, 2, 419−436

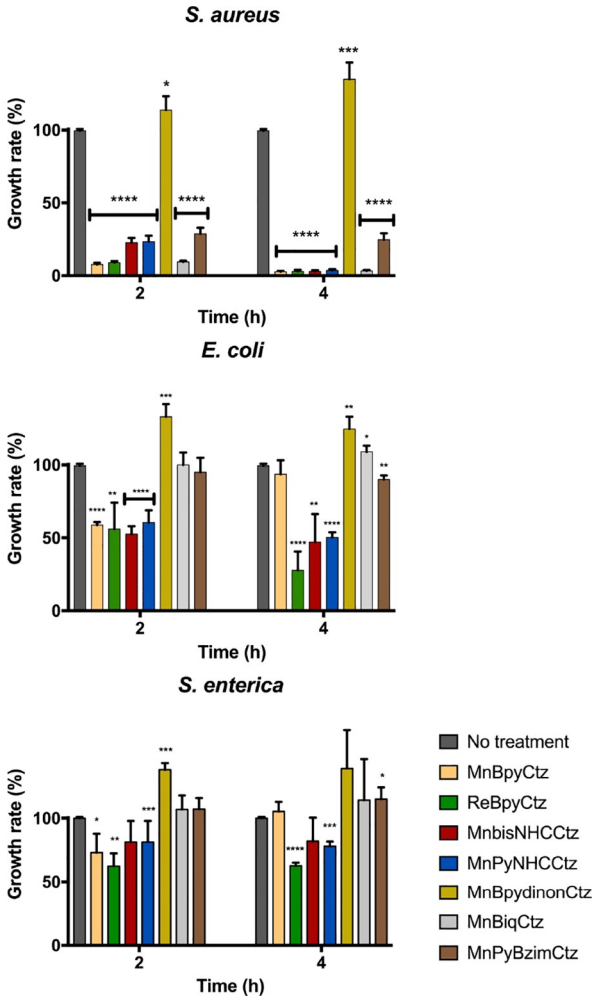

Figure 3. *S. aureus* cells are sensitive to conjugated CORMs. Cells of *S. aureus* MRSA, *E. coli* MG1655, and *S. enterica* SL1344 were treated with the indicated CORMs (35 μM for Gram-negative bacteria and 10 μM for *S. aureus*). The percentage of the growth rate was determined in relation to untreated cells collected at 2 h and 4 h. Data represent the average of three independent biological samples, with error bars representing the standard deviation. *P < 0.05, **P < 0.01, ***P < 0.001, and ****P < 0.0001.

bidentate N−N, N−C, and C−C ligands. Given the similarity of the electronic properties suggested by the relatively close νCO values and the chemical stability revealed in the blood tests (see below), it seems that the fine structural details of the ancillary ligands are key to controlling the activity of the CORMs against *S. aureus*. The Re and Mn isostructural analogues (**MnBpyCtz** and **ReBpyCtz**, respectively) present a flat and compact bipyridyl ligand attached to the $[M(CO)_3(Ctz)]^+$ fragment. When compared with cells not exposed to bacteria, cells had their growth decreased to *ca.* 8 and 2% at 2 and 4 h after the challenge, respectively. Increasing the bulk of the bipyridyl ligand at the distal side to the metal, that is, the 4 and 4′ positions of the ring, completely prevents activity, making **MnBpydinonCtz** innocuous. The presence of CH_3 or CO_2CH_3 groups at the 4 and 4′ positions of bipyridyl also decreases the antimicrobial effect, as previously reported.[15] This is due to a steric effect since the electronic effects of nonyl and carboxyl substituents are opposed, yet the antimicrobial activity follows in the same direction.

The superior activity of the small, compact, and unencumbered Bpy derivatives led us to explore other $[M(CO)_3(L-L)(Ctz)]^+$ complexes with bidentate L−L ligands structurally similar to 2,2′-bipyridyl. Biq was an obvious choice, and in fact, complex **MnBiqCtz** significantly limited *S. aureus* growth, much like the effect of 2,2′-bipyridyl derivative **MnBpyCtz**. The larger occupation of the equatorial plane of conjugate **MnBiqCtz** by the extended π-ligand was no significant impediment to the CORM activity. On the contrary, a smaller yet asymmetrical occupation of the equatorial plane had an important effect, lowering the antibacterial activity of **MnPyBzimCtz** in comparison to that of **MnBiqCtz** and **MnBpyCtz**. The growth of *S. aureus* in the presence of **MnPyBzimCtz** did not increase significantly with time, remaining similar at 2 and 4 h postexposure. It also emerged that the bipyridine and biquinoline complexes are more active at short incubation times than all other compounds tested. Complexes **MnPyNHCCtz** and **MnbisNHCCtz** that feature NHC ligands are also very active, but their action is markedly slower than that of the Bpy and Biq derivatives. The fact that the bis-NHC ligand in **MnbisNHCCtz** is not flat, unlike the PyNHC ligand in **MnPyNHCCtz**, does not make any difference in the activity profile of both complexes.

The antibacterial potency of the clotrimazole-free $[M(CO)_3(L-L)Br]$ precursor complexes was also checked against the same bacteria. As shown in Supporting Information Table S2, the halide complexes $[M(CO)_3(L-L)Br]$ (M = Mn and Re), **MnBpyBr** and **ReBpyBr**, that are the precursors to **MnBpyCtz** and **ReBpyCtz**, respectively, exhibited MICs > 32 μg/mL for all bacteria and percentages of growth higher than 90%. This lack of bactericidal activity for the halide complexes was also reported by Sovari *et al.*[19] A similar behavior was observed for complexes $[Mn(CO)_3(L-L)X]$ (X = Br and I), **MnPyNHCI** and **MnbisNHCBr**, which are the precursors of **MnPyNHCCtz** and **MnbisNHCCtz**, respectively. The ligands of the most potent CORM−Ctz conjugates, namely, bipyridyl, and the NHC cationic precursors of the ligands in **MnPyNHCCtz** $[(PyNHC^{Me})\cdot HI]$ and **MnbisNHCCtz** $[(bisNHC^{Me})\cdot 2(HBr)]$ did not affect bacterial growth. Bipyridyl, though, was moderately active against *E. coli* and *S. enterica* at 250 μM, inhibiting their growth to *ca.* 50−60% after 4 h of exposure, but there was no effect on *S. aureus*.

In summary, we conclude that antimicrobial activity of the conjugates is dependent on the presence of the clotrimazole ligand, which, in its free form, is nontoxic to *E. coli* and *S. enterica* and moderately active against *S. aureus*. The fact that compounds **MnBpyCtz**, **ReBpyCtz**, **MnBiqCtz**, **MnPyNHCCtz**, and **MnbisNHCCtz** are significantly more potent against *S. aureus* than clotrimazole alone demonstrates that some kinds of $[M(CO)_3(L-L)]^+$ fragments are able to substantially enhance Ctz's antibacterial activity.

CORM−Clotrimazole Conjugates Are Not Cytotoxic at the MIC Concentration

When conjugating clotrimazole to a rhenium-based CORM, toxicity dosage to human hepatic (HepG2) and porcine kidney (LLC-PK1) cell lines decreases. Half-maximum inhibitory concentration (IC_{50}) values for **ReBpyBr** and clotrimazole are 10−30 times higher than the IC_{50} values of **ReBpyCtz** (Table 2).

https://doi.org/10.1021/acsbiomedchemau.2c00007
ACS Bio Med Chem Au 2022, 2, 419−436

Table 2. Half-Maximum Inhibitory Concentration (IC_{50}) Expressed in Micromolar[a]

	HepG2 IC_{50} (μM)	LLC-PK1 IC_{50} (μM)
ReBpyCtz	1.4 ± 0.4	2.0 ± 0.8
ReBpyBr	31.1 ± 11.0	16.4 ± 8.3
Ctz	29.2 ± 21.9	11.6 ± 3.2

[a]IC_{50} values of **ReBpyCtz**, **ReBpyBr**, and clotrimazole were determined for human hepatic (HepG2) and porcine kidney (LLC-PK1) cell lines.

CORM–Clotrimazole Conjugates Are Stable Complexes in Blood and Release CO into Bacteria

In vivo, antibiotic molecules must reach the target bacterial cells intact, resisting chemical attack and decomposition caused by blood components, namely, serum albumin and hemoglobin. Serum albumin can radically modify and hijack the coordination sphere of CORMs bearing labile ligands, as in the case of CORM-3 and other *fac*-{$Ru(CO)_3$}d^6-based CORMs.[6,23] Hemoglobin can rapidly scavenge labile CO ligands from many CORMs, forming carboxyhemoglobin (COHb) and accelerating their irreversible decomposition, as in the case of [$Mo(CO)_3$(histidinate]Na (ALF186).[24] If CO is involved in the killing mechanism, as is expected from a CORM, such scavenging inhibits its activity.[2,25] For all these reasons, testing the stability of CORM conjugates is an essential step in their characterization and was performed for the more active complexes, namely, **MnBpyCtz**, **ReBpyCtz**, **MnBiqCtz**, **MnPyBzimCtz**, **MnPyNHCCtz**, and **MnbisNHCCtz**.

For this purpose, solutions of CORMs were added to sheep whole blood in Alsever's solution, and the blood parameters were read in a blood oximeter at 15 min intervals for 1 h, as previously described.[24] The value of COHb for all complexes remained at the level of the control (Figure 4A). Also, the value of %Met-Hb remained unchanged throughout the experiment (Figure 4B). The COHb values did not change, showing that the CORM conjugates do not decompose in blood. Simultaneously, the %Met-Hb value remained unaltered (Figure 4B). These effects were confirmed in the control experiment carried out with the weak bactericidal complex [$Mn(CO)_5Br$] (ALF021) that generates CO to increase %CO-Hb already at the time of mixing and until *ca.* 30 min postincubation, while the %Met-Hb decreases relative to the control (Figure 4C,D). The instability of [$Mn(CO)_5Br$] in blood is readily understood considering the well-known lability of two CO ligands of [$Mn(CO)_5X$] complexes to form kinetically stable *fac*-[$Mn(CO)_3$]$^+$ derivatives similar to those found in our CORM conjugates. The reducing effect that decreases %Met-Hb is unavoidable for CORMs bearing metals in low oxidation states, as in the case of Mn(I).[26]

To analyze CO release into bacterial cells, *S. aureus* was exposed to active CORM conjugates and COP-1, a probe that forms with CO a fluorescent carbonylation product.[27] Figure 4E shows that these complexes release CO into *S. aureus*, while cells treated with the clotrimazole-free precursors of **MnBpyCtz** and **ReBpyCtz**, namely, **MnBpyBr** and **ReBpyBr**, respectively, did not present significant COP-1 fluorescence (Supporting Information Figure S1).

Altogether, we concluded that all [$M(CO)_3$(L–L)(Ctz))]$^+$ conjugates are stable in blood under normoxic conditions, meaning that their CO load is not scavenged by the hemoglobin in circulation. Furthermore, these conjugated CORMs are capable of releasing CO inside bacterial cells.

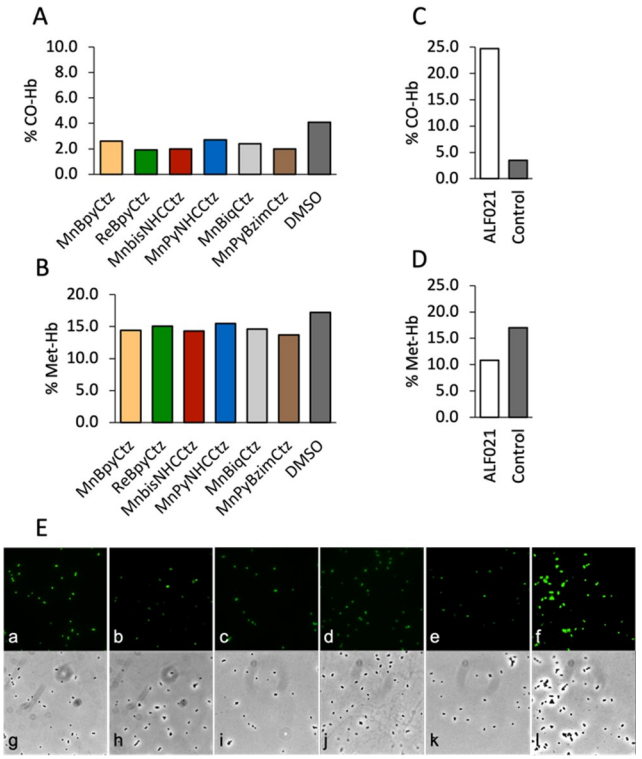

Figure 4. Release of CO from conjugated CORMs into blood and bacteria. (A) Percentage of CO–hemoglobin formed in blood samples incubated, for 1 h, with **MnBpyCtz**, **ReBpyCtz**, **MnbisNHCCtz**, **MnPyNHCCtz**, **MnBiqCtz**, **MnPyBzimCtz**, and DMSO. (B) Percentage of Met–hemoglobin formed in blood samples incubated for 1 h with **MnBpyCtz**, **ReBpyCtz**, **MnbisNHCCtz**, **MnPyNHCCtz**, **MnBiqCtz**, **MnPyBzimCtz**, and DMSO. (C) Percentage of CO–hemoglobin bound in blood samples incubated, for 30 min, with ALF21. (D) Percentage of Met–hemoglobin bound in blood samples incubated, for 30 min, with ALF21. (E) Fluorescence microscopy images of *S. aureus* MRSA CORM–Ctz conjugates (10 μM, 15 min) and incubated with the fluorescent probe COP-1. Representative images of fluorescent cells treated with **MnBpyCtz** (a), **ReBpyCtz** (b), **MnbisNHCCtz** (c), **MnPyNHCCtz** (d), **MnBiqCtz** (e), and **MnPyBzimCtz** (f) (upper row) and their corresponding bright field images (g, h, i, j, k, and l, respectively) (lower images). The population values correspondent to fluorescent green cells represented on the images are 80% (a), 74% (b), 84% (c), 44% (c), 86% (d) and 85% (e), respectively. At least 300 cells, from at least three independent experiments, were analyzed for each condition.

MoA Study

Among the set of Ctz conjugates analyzed in this study, **ReBpyCtz** was selected as the prototype for further mechanism of action (MoA) studies due to its high antibacterial activity. In all MoA investigations, **ReBpyCtz** was evaluated alongside the two molecules that represent its two components, that is, Ctz and **ReBpyBr**, to unravel which precursor conveyed which characteristics to the resulting hybrid.

Spectrum of Bacterial Target Species. In order to evaluate their target spectrum, we first tested the three molecules against a broader range of bacterial species, including well-characterized model species and a panel of ESKAPE pathogens.[28] MIC values are presented in Table 1.

https://doi.org/10.1021/acsbiomedchemau.2c00007
ACS Bio Med Chem Au 2022, 2, 419–436

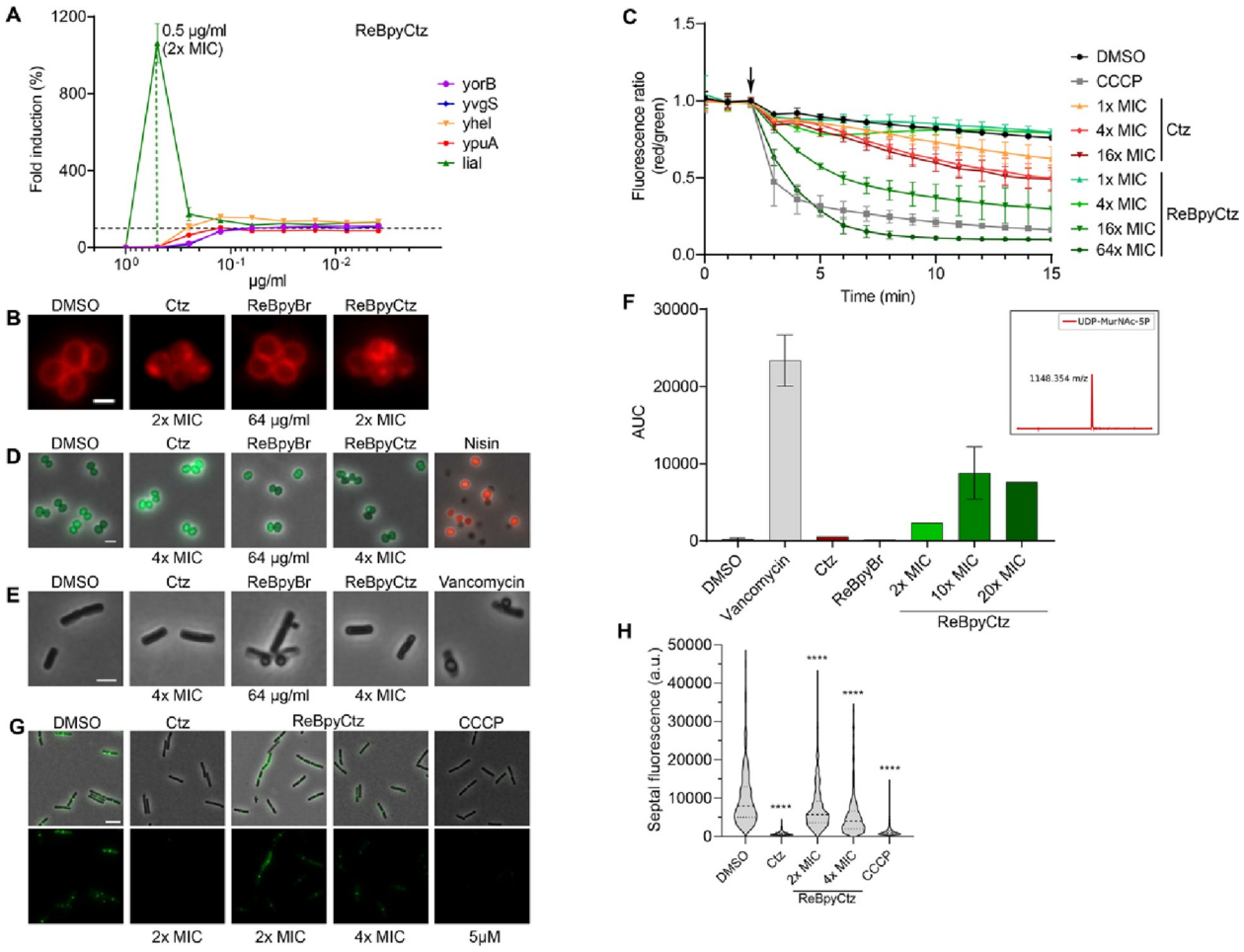

Figure 5. Effect of **ReBpyCtz** on the cell envelope of growing *B. subtilis* and *S. aureus* cells. (A) Firefly luciferase bioreporter profiling demonstrates *liaI* promotor induction by **ReBpyCtz**. The *liaI* promotor responds to cell envelope damage and particularly to agents interfering with cycling of the membrane-standing undecaprenyl-P precursor. Luminescence values recorded at a single predetermined time point after **ReBpyCtz** addition (see the Material and Methods section) were normalized to the untreated control (100%, black, horizontal dashed line) and plotted against the concentration of **ReBpyCtz**. At the MIC, the *liaI* bioreporter is induced, while the signals for the noninduced bioreporters fall below the background level, indicating impaired biosynthetic capacity. The corresponding experiments for Ctz, **ReBpyBr**, and reference antibiotics are shown in Supporting Information Figure S2. Error bars represent the SD of two biological replicates (*i.e.*, cultures grown and treated independently on different days) with two technical replicates per test day. (B) **ReBpyCtz** and Ctz disturb the topology of the cytoplasmic membrane. Membrane staining by FM 5-95 of *S. aureus* NCTC 8325 treated for 30 min with Ctz (8 μg/mL, 2× MIC), **ReBpyBr** (64 μg/mL), and **ReBpyCtz** (0.5 μg/mL, 2× MIC) compared to the negative control treated with DMSO. Scale bar, 1 μm. One experiment representative of three biological replicates is shown. (C) Time-resolved effect of Ctz and **ReBpyCtz** on the membrane potential of *S. aureus* NCTC8325 measured by $DiOC_2$ (3) staining in relation to the respective MICs. Protonophore CCCP (5 μM, 0.4× MIC) was used as a positive control and DMSO as a negative control. The arrow indicates the time point of compound addition. Four biological replicates and SD are presented. (D) Membrane integrity is not severely affected. Exposure of *S. aureus* NCTC8325 to either Ctz (16 μg/mL, 4× MIC), **ReBpyCtz** (1 μg/mL, 4× MIC), or **ReBpyBr** (64 μg/mL) for 120 min, followed by staining with membrane-permeant Syto9 (green) and membrane impermeant PI (red). Nisin (100 μg/mL) served as a positive control and DMSO (1%) as a negative control. Merged overlay of three photographs of the same cells acquired in the brightfield, green, or red fluorescence channel. Scale bar, 2 μm. (E) **ReBpyBr** leads to membrane blebbing in *B. subtilis* 168, indicative of peptidoglycan weakening. Bright-field visualization of the formation of blebs after 30 min treatment with **ReBpyBr** (64 μg/mL) or vancomycin (Van, positive control, 2 μg/mL). No blebs were induced by Ctz (8 μg/mL, 4× MIC), **ReBpyCtz** (1 μg/mL, 4× MIC), or DMSO (1%, negative control). Scale bar, 2 μm. (**F**) UDP-MurNAc-pentapeptide accumulation in *S. aureus* ATCC 29213 after 30 min of treatment with DMSO (negative control), vancomycin (2 μg/mL, 8× MIC, positive control), Ctz (40 μg/mL, 10× MIC), **ReBpyBr** (64 μg/mL), or **ReBpyCtz** (0.5, 2.5, and 5 μg/mL, corresponding to 2×, 10×, and 20× MIC, respectively) shown as AUC values of EICs. An exemplary EIC (shown for the **ReBpyCtz** at 10× MIC sample) is presented as an inset, depicting the mass of UDP-MurNAc-pentapeptide (m/z = 1148.354) measured in the negative ionization mode. Further EICs and corresponding total ion chromatograms are presented in Supporting Information Figure S5. (G) Monitoring nascent peptidoglycan in growing *B. subtilis* cells. HADA labeling of *B. subtilis* 168 after 5 min exposure to Ctz (4 μg/mL, 2× MIC), **ReBpyCtz** (0.5 μg/mL, 2× MIC or 1 μg/mL, 4× MIC), or CCCP (5 μM) compared to DMSO (0.5%), the negative control. Fluorescence channel (bottom) and overlay with the phase contrast (top). Microscopic settings were selected to yield a good signal in the DMSO control and then kept constant for all micrographs. Scale bar, 5 μm. (H) Quantification of (G). The violin plots represent the relative septal HADA intensities quantified from ≥100 cells per experiment from three independent biological replicates; ****P < 0.0001.

ReBpyCtz inhibited the Gram-positive representatives of the panel (*Bacillus subtilis*, *S. aureus*, and *Enterococcus faecium*) with MICs of 0.25−2 μg/mL (0.27−2.2 μM) and the Gram-negative Enterobacteriaceae and nonfermenters with MICs of

https://doi.org/10.1021/acsbiomedchemau.2c00007
ACS Bio Med Chem Au 2022, 2, 419−436

8−32 μg/mL (8.7−34.7 μM). While Ctz on its own possessed moderate antibacterial activity (MIC 2−8 μg/mL; 5.8−23.2 μM) against the Gram-positive species only, the conjugated compound **ReBpyCtz** proved significantly more potent and also showed moderate activity against Gram-negative strains. Organometallic precursor **ReBpyBr** did not yield an MIC up to the highest concentration tested (32 μg/mL; 64 μM). In all following MoA studies, the concentration range was adjusted to their respective MIC levels to correlate the observed biological activities directly to cell death.

Bioreporter Profiling. To obtain an unbiased first impression of the kind of stress bacterial cells feel when exposed to **ReBpyCtz**, Ctz, and **ReBpyBr**, we used a bioreporter panel based on the sensitive reference strain *B. subtilis* 168, designed to specifically sense and signal interferences with most metabolic pathways commonly affected by antibiotics.[29,30]

The readout was based on the induction of the firefly luciferase cloned behind the promoters of genes *yorB*, *helD*, *bmrC*, *ypuA*, or *liaI*, which were previously shown to specifically signal the following kinds of damage: P_{yorB} (interference with the DNA synthesis or structure); P_{helD} (interference with RNA synthesis); P_{bmrC} (stalling of ribosomal translation); P_{ypuA} (diverse kinds of stress affecting the cell wall or membrane); and P_{liaI} (cell envelope stress, particularly interference with cycling the membrane standing lipid carrier undecaprenyl-phosphate). While Ctz and **ReBpyBr** gave no signal in this assay, **ReBpyCtz** strongly induced P_{liaI} at a concentration of 0.5 μg/mL (2× MIC) (Figure 5A and Supporting Information Figure S2), suggesting an attack on the cytoplasmic membrane and, furthermore, potential interference with peptidoglycan synthesis.

Effects on the Topology, Functionality, and Integrity of the Cytoplasmic Membrane. Next, we monitored the distribution of the membrane dye FM 5-95 after treatment with Ctz, **ReBpyBr**, and **ReBpyCtz**. FM 5-95 is a lipophilic dye, which stained the entire cytoplasmic membrane of a dimethyl sulfoxide (DMSO)-treated control aliquot of *S. aureus* NCTC8325 with homogeneous red fluorescence. The addition of **ReBpyCtz** and Ctz close to their respective MICs triggered a spotty phenotype, demonstrating dye rearrangement and aggregation and suggesting a general disturbance of the membrane topology (Figure 5B).

Exploring the membrane defect further, we investigated the effect of **ReBpyCtz** on the membrane potential of *S. aureus* NCTC8325 using fluorescence spectroscopy with dye 3,3′-diethyloxacarbocyanine iodide [$DiOC_2(3)$]. When entering the cell, the green fluorescence of $DiOC_2(3)$ shifts toward a red emission, due to self-association of the dye molecules. The degree of self-aggregation, and thus the extent of the green-to-red shift, depends on the membrane potential. **ReBpyCtz** reduced the membrane potential of *S. aureus* significantly and reproducibly, although comparably high compound concentrations were required (Figure 5C and Supporting Information Figure S3). A slight effect emerged at 4× MIC and increased in a concentration-dependent manner, but only at 64× MIC did the impact of **ReBpyCtz** match the strength of the effect that protonophore carbonyl cyanide *m*-chlorophenylhydrazone (CCCP) already yielded at 0.4× MIC (Supporting Information Figure S3). Consequently, it is highly unlikely that membrane depolarization is the cause of **ReBpyCtz**-mediated bacterial death. Ctz did also reduce the membrane potential, while **ReBpyBr** showed no effect.

We also investigated the integrity of the cytoplasmic membrane. *S. aureus* NCTC8325 was simultaneously exposed to two fluorescent dyes, cell-permeant SYTO9 and membrane non-permeant, positively charged propidium iodide (PI). The latter can cross the bacterial cytoplasmic membrane only if pores or other gross membrane inhomogeneities emerge, and when this occurs, PI inserts into the DNA, thereby emitting red fluorescence. None of the three agents (at 4× MIC for Ctz and **ReBpyCtz** and at 64 μg/mL for **ReBpyBr**) allowed for the passage of PI through the membrane, excluding extensive impairment of the membrane barrier function in all three cases (Figure 5D and Supporting Information Figure S4).

Impact on Peptidoglycan Biosynthesis. As the induction of the *liaI* bioreporter strain had signaled potential impairment of peptidoglycan synthesis, we also investigated the integrity of the peptidoglycan sacculus. Antibiotics weakening the peptidoglycan sacculus, such as the transglycosylation inhibitor vancomycin, are known to cause membrane extrusions through holes in the peptidoglycan meshwork, when cells are subjected to a fixation procedure with acetic acid/methanol.[31] Unexpectedly, we observed the same phenotype clearly and repeatedly for **ReBpyBr** at 64 μg/mL, but neither for **ReBpyCtz** nor for Ctz (Figure 5E). This result indicates that although the **ReBpyBr** precursor was not potent enough to yield an MIC, it did possess a bioactivity related to peptidoglycan metabolism.

Inhibitors of membrane-associated stages of peptidoglycan synthesis commonly induce the accumulation of the ultimate soluble peptidoglycan precursor UDP-*N*-acetylmuramic acid-pentapeptide (UDP-MurNAc-PP) in the bacterial cytoplasm. Therefore, we next analyzed the cytoplasmic level of this metabolite in treated cells. Indeed, **ReBpyCtz** led to a strong induction of UDP-MurNAc-PP, and the accumulation was already significant at 2× MIC (Figure 5F), suggesting that inhibition of peptidoglycan synthesis contributes to the antibacterial effect of **ReBpyCtz**. The strong accumulation of UDP-MurNAc-PP was a new characteristic of the **ReBpyCtz** conjugate, which was not shown by either **ReBpyBr** or Ctz. The fact that UDP-MurNAc-PP could accumulate supports the experiments described above. Precursor biosynthesis requires energy, in line with the observed lack of major membrane depolarization at low multiples of the MIC. It also precludes the presence of membrane pores through which the peptidoglycan precursor UDP-MurNAc-PP, ions, and further cytoplasmic content would leak out.

A disturbance of the peptidoglycan synthesis process was also suggested by a pulse-labeling experiment with fluorescent 7-hydroxycoumarincarbonylamino-D-alanine (HADA). HADA allows us to monitor sites of nascent peptidoglycan synthesis and murein remodeling activities in living bacterial cells by its incorporation into the fifth position of the stem peptide by D,D-transpeptidases in vegetative *B. subtilis* cells.[32] In untreated *B. subtilis* cells, the label was most clearly visible at the septa, in accordance with the high peptidoglycan synthetic activity known for the septal region and the corresponding abundance of D-Ala−D-Ala moieties.[33] Exposure of *B. subtilis* cells to **ReBpyCtz** and Ctz clearly affected HADA incorporation. Comparing the effects of both agents side by side at corresponding multiples of the MIC, it emerged that Ctz inhibited HADA incorporation more rapidly and strongly than **ReBpyCtz** (Figure 5G,H). The immediate phenotype induced by Ctz was reminiscent of the one induced by the uncoupler CCCP. **ReBpyBr** did not inhibit HADA incorporation even

https://doi.org/10.1021/acsbiomedchemau.2c00007
ACS Bio Med Chem Au 2022, 2, 419−436

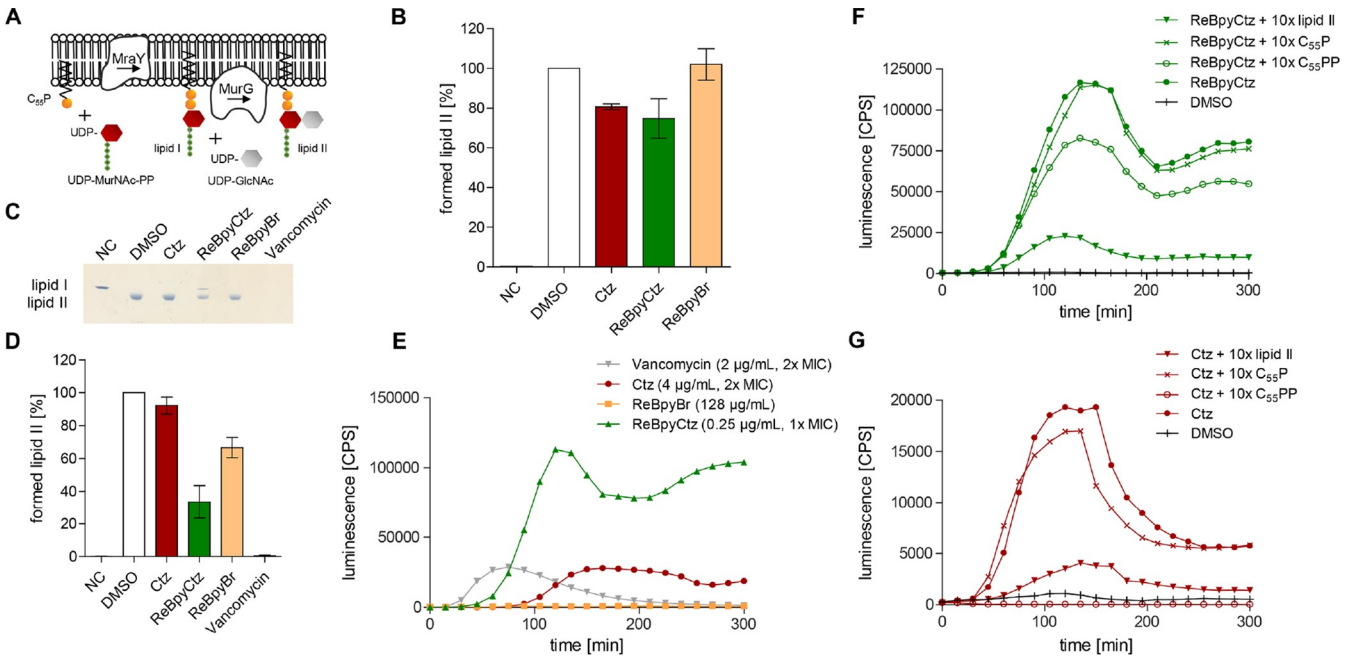

Figure 6. Inhibition of *in vitro* peptidoglycan synthesis by **ReBpyCtz** and interaction with peptidoglycan precursors. (A) Schematic of lipid II synthesis in *S. aureus* NCTC8325. UDP-MurNAc-PP and lipid carrier C55P are used as substrates for lipid I synthesis by MraY. MurG catalyzes the addition of GlcNAc from UDP-GlcNAc, yielding lipid II. (B) Influence of **ReBpyCtz**, **ReBpyBr**, and Ctz on lipid II synthesis using MraY- and MurG-containing membrane preparations of *Micrococcus luteus*. At a 10-fold molar excess over C55P, **ReBpyCtz** and Ctz slightly reduced the amount of lipid II formed, while **ReBpyBr** did not. NC, negative control, reaction mixture without membranes; DMSO (1%). Error bars represent the SD of two replicates. (**C**) Influence of **ReBpyCtz** on lipid II synthesis from purified lipid I (2 nmol) and UDP-GlcNAc by purified MurG. Test compounds were applied in DMSO (1%) at a 10-fold molar excess over lipid I. TLC curves showing the extracted lipids at the end of the reaction. Vancomycin was used as an inhibition control; its binding to lipid I retains the complex in the aqueous phase and prevents it from being extracted. **ReBpyCtz** sightly inhibited the conversion of lipid I to lipid II. (D) Quantification of the bands visible on the TLC plate in (**C**). **ReBpyCtz** inhibits the MurG reaction. Error bars represent the SD of two replicates. (E) LiaI lux bioreporter strain based on the *Photorhabdus luminescens* luciferase system, yielding a continuous fluorescence signal. The *liaI* promotor in *B. subtilis* 168 is induced upon treatment with **ReBpyCtz** and Ctz around their respective MIC levels, albeit to different extents. No induction was observed for **ReBpyBr**. Vancomycin (2 µg/mL, 2× MIC) served as a positive control. (F,G) Antagonization of the bioreporter induction by peptidoglycan precursor addition. In the case of **ReBpyCtz** (F), purified lipid II (triangles) antagonized the most effectively, and in the case of clotrimazole (G), C55PP antagonized the best. C55P was not significantly effective. The depicted experiment is representative of two independent biological replicates.

after longer CORM exposure (Supporting Information Figure S6). This observation implied a divergent molecular impact of **ReBpyCtz** and Ctz on cell physiology and the peptidoglycan synthesis process, a hypothesis that we investigated further in *in vitro* peptidoglycan synthesis assays (Figure 6).

The fact that **ReBpyCtz** had triggered a prominent accumulation of the ultimate cytoplasmic peptidoglycan precursor UDP-MurNAc-PP suggested a blockade at a later stage of peptidoglycan biosynthesis. Therefore, we focused our follow-up experiments on the membrane-associated stages of this pathway (Figure 6A) and, in particular, on the reactions leading to the membrane-standing precursors undecaprenyl-pyrophosphate-MurNAc-PP (lipid I) and undecaprenyl-pyrophosphate-MurNAc-PP-*N*-acetyl glucosamine (lipid II). In a first step, using a crude membrane preparation of *Micrococcus luteus* (Figure 6B), we studied the formation of lipid II from soluble precursors UDP-MurNAc-PP and UDP-GlcNAc and membrane carrier $C_{55}P$ in a coupled reaction series that involved the MraY and MurG enzymes contained in the membrane. Here, **ReBpyCtz** showed a slight but reproducible trend of inhibition of lipid II formation. Next, we split the metabolic cascade into the individual enzyme reactions using purified, recombinant enzymes and purified substrates. The MurG-mediated conversion of lipid I to lipid II was clearly inhibited by **ReBpyCtz** (Figure 6C,D), while the MraY-mediated formation of lipid I was not affected (Supporting Information Figure S7).

Inhibition of the MurG reaction can occur by direct interference with the catalytic function of the enzyme or by steric hindrance through sequestration of the peptidoglycan precursor serving as a substrate. To test if **ReBpyCtz** can bind to peptidoglycan precursors, we used another bioreporter strain. The luciferase of *Photorhabdus luminescens* yields a continuous light signal, and fused to the *liaI* promotor, it is a sensitive sensor of an interference of an agent with the lipid II cycle.[34] **ReBpyCtz** strongly induced this bioreporter strain at 1× MIC (Figure 6E and Supporting Information Figure S8). Capitalizing on this stable signal, we tested if the external addition of certain peptidoglycan precursors to the reporter strain might be capable of antagonizing the **ReBpyCtz**-triggered signal. Indeed, when purified lipid II was added to the supernatant of the bioreporter assay mixture, it prevented **ReBpyCtz** from eliciting the *liaI* stress response in the bioreporter strain (Figure 6F). The explanation is that lipid II supplemented to the medium forms a complex with **ReBpyCtz**, thereby preventing the CORM conjugate from binding to the native lipid II in the *B. subtilis* cell membrane. **ReBpyCtz** clearly displayed its potential to bind lipid II and also to a lesser extent $C_{55}PP$. In contrast, Ctz showed the

https://doi.org/10.1021/acsbiomedchemau.2c00007
ACS Bio Med Chem Au 2022, 2, 419−436

highest affinity for C_{55}PP (Figure 6G), suggesting that **ReBpyCtz** and Ctz have a different molecular binding mode.

DISCUSSION

Most of the so-far reported CORMs derived from the *fac*-{$M(CO)_3$}d^6 fragment (M = Mn and Re) only reveal biological activity, and in particular antibacterial activity, when irradiated to promote the release of CO.[10,35−37] In contrast, complex **MnBpyCtz** is active without irradiation and stands out for its high activity against Gram-positive bacteria. Particularly interesting is the fact that its bactericidal activity exceeds that of its clotrimazole ligand.[16]

As these characteristics posed several questions, including the contribution of CO to the enhanced antibacterial activity of **MnBpyCtz** when compared to free Ctz, we synthesized compounds with various modifications relative to the structure of **MnBpyCtz** and studied their antibacterial potency. The complexes have the general formulation $[M(CO)_3(L{-}L)(Ctz)][OTf]$, where M = Mn and Re and L−L are bidentate N−N, N−C, and C−C ligands. All the N−N ligands are diimines based on N-heterocyclic rings. The C ligands are imidazolidenes or NHC. All complexes are positively charged, have the same triflate counterion, and cover a continuum of electronic density at the metal that places the ν_{sym}CO vibrations between 2038 cm^{-1} (for **MnBpyCtz**) and 2013 cm^{-1} for **MnbisNHCCtz**.

The overall data indicate that **MnBpyCtz** and its analogue **ReBpyCtz** are active against Gram-positive bacteria, and the introduction of bulky substituents on the Bpy ligand cancels or strongly impairs the bactericidal activity. The substitution of Bpy with biquinoline or other small bicyclic ligands with N(sp^2) or C(sp^2) binding atoms such as py-imidazolidene or bis-imidazolidene also leads to highly active clotrimazole conjugates. The fact that the pyridine-benzimidazole ligand in **MnPyBzimCtz** causes an intermediate effect suggests that there is a net stereochemical component driving the activity of this family of complexes. Electronic factors do not seem to play any role as the activity of **MnBpyCtz**, with the lower electronic density (highest ν_{sym}CO), is close to that of the very electron rich bis−carbene complex **MnbisNHCCtz** (lowest ν_{sym}CO).

The presence of the clotrimazole ligand is necessary, though not sufficient, to achieve antibacterial activity of the conjugates. Indeed, while **MnBpyCtz**, **ReBpyCtz**, **MnBiqCtz**, **MnPyNHCCtz**, and **MnbisNHCCtz** are much more active than clotrimazole alone, conjugate **MnPyBzimCtz** is less active than free Ctz, and **MnBpydinonCtz** lacks activity. Since all of these conjugates share a common $[M(CO)_3(Ctz)]^+$ fragment and neither the metal nor their ligand-controlled electronic properties play a role, we are compelled to assume that the structural properties of the bidentate L−L ligands are the main determinant of activity. However, the structural properties of the precursors do not per se confer activity as none of the conjugate precursors with the formula $[M(CO)_3(L{-}L)Br]$ revealed any bactericidal activity, regardless of the nature of the L−L ligand. This result suggests that the lack of a positive charge in these organometallic precursors hinders their interaction with the bacterial cells, rendering them inactive. Indeed, all Ctz conjugates bear a positive charge that by itself is not a sufficient condition for potent antibacterial activity, as that of conjugate MnBpydinonCtz demonstrates. The positive charge effect is well-recognized to be strongly implicated in the mechanism of many antibacterial agents including $[Re(CO)_3(L_3]^+$ derivatives.[13,38,39] Although electronic properties do not appear to be determinants of the antibacterial activity as such, they can still play a role in determining the chemical stability of the conjugates and hence in the release of CO. Since we observed that none of the conjugates decomposed in whole blood, that is, in the presence of plasma proteins and erythrocytes, under normoxic conditions, we must acknowledge their significant stability in biological media.

In contrast to the literature examples already mentioned above,[10,36,37] light irradiation is not necessary to trigger a bactericidal effect in clotrimazole conjugates, and CO is released into *S. aureus* cells treated with **MnBpyCtz**, **ReBpyCtz**, **MnBiqCtz**, **MnPyBzimCtz**, **MnPyNHCCtz**, and **MnbisNHC**. The stability toward CO release demonstrated by these conjugates in normoxic blood and the absence of the need for photochemical decomposition support the notion that the conjugates enter the bacterial cells structurally intact and only decompose to release CO once attacked by the cell's chemical machinery.

The contribution of CO to the bactericidal activity of CORMs is well-established through binding and impairment of essential bacterial heme proteins, such as those of the respiratory chain.[40,41] Moreover, evidence has accumulated that CO inhibits not only heme proteins but also iron proteins.[42−44] Previous studies showed that the cationic photoCORM $[Mn(CO)_3(\kappa^3\text{-tpa})]Br$ is not internalized, and its killing effect is driven by the CO released upon irradiation and diffusion into the cells. Meanwhile, the Mn scaffold of the photoCORM remaining outside of the cell generates highly toxic HO radicals through the reaction with the H_2O_2 that leaks from the cell.[11] In contrast, our present study demonstrates that bactericidal Ctz−CORM conjugates enter the bacterial membrane.

The clotrimazole ligand bestows a new quality to the CORMs, enabling their membrane insertion and potentially even passage into the cytoplasm. Nevertheless, the conjugated Ctz−CORM **ReBpyCtz** is more than the sum of its parts. Although precursor **ReBpyBr** has no antibacterial activity and Ctz shows only moderated MICs, the potency of **ReBpyCtz** is 1 order of magnitude higher than that of Ctz, while its spectrum of bacterial target species is expanded toward Gram-negative bacteria. In general, the activity of **ReBpyCtz** is higher against Gram-positive bacteria than against Gram-negative bacteria, in accordance with the high molecular weight of the compound (920 g/mol) and the resulting difficulties in crossing the Gram-negative outer membrane. When **ReBpyCtz** is added to *S. aureus* cells, the topology of the cytoplasmic membrane is immediately and severely disturbed. The rapid aggregation of the FM 5-95 dye in large clusters is probably just a direct illustration of what may be happening to various other membrane components that can no longer take their normal positions and are prevented from their normal interactions. The membrane potential dissipates, although severe depolarization only takes place at concentrations well above the MIC, indicating that membrane depolarization is not the primary cause of cell death. There is no indication of prominent pores in the cytoplasmic membrane of *S. aureus*, as the cell's intake of the PI dye was still precluded after 2 h of treatment at 4× MIC.

Apart from a general impact on the membrane topology and energy functions, **ReBpyCtz** demonstrated inhibitory effects on peptidoglycan biosynthesis in several independent assays. The *liaI* promotor was strongly induced, known to prominently signal disturbance by compounds that interfere

https://doi.org/10.1021/acsbiomedchemau.2c00007
ACS Bio Med Chem Au 2022, 2, 419−436

with cycling of the undecaprenyl precursor in peptidoglycan biosynthesis ("lipid II cycle").[34] Accordingly, the ultimate cytoplasmic peptidoglycan precursor UDP-MurNAc-pentapeptide accumulated in the cytoplasm of treated cells. Dissecting the peptidoglycan synthesis pathway via *in vitro* assays with purified enzymes and substrates revealed that **ReBpyCtz** inhibited the MurG-mediated conversion of lipid I to lipid II but not the preceding MraY-mediated formation of lipid I, indicating a marked preference for the MurG reaction. Effective antagonization of the *liaI* stress response via the addition of external lipid II indicates that **ReBpyCtz** has the potential to bind to lipid-bound peptidoglycan precursors, and the binding affinity was higher for lipid II than for C_{55}PP. The observed inhibition of the MurG reaction *in vitro* implies that lipid I is also recognized and bound, thus offering a rationale for the inhibition of the reaction by substrate complexation rather than by direct enzyme inactivation. A further indication for lipid I binding is the result that the reaction product lipid I accumulated in the MraY assay as a result of shifting the reversible enzyme reaction to the product side.

Contemplating the main cause of the bacterial death, our data show that *B. subtilis* and *S. aureus* cells signal a disturbance of peptidoglycan synthesis already close to the MIC (0.5−2× MIC), as evidenced by the bioreporter studies and UDP-MurNAc-PP accumulation, respectively, while prominent membrane potential depolarization requires higher concentrations. At 4× MIC, the membrane potential of **ReBpyCtz** is only transiently reduced, and 16× MIC is required for a permanent effect. It is also noteworthy that none of the other bioreporters, covering a broad range of classical antibiotic target areas, gave a signal. Therefore, it seems likely that inhibition of peptidoglycan synthesis contributes to the killing of bacterial cells by **ReBpyCtz**. However, the strong aggregation of dye molecules in the membrane that starts within minutes of compound addition is not a typical feature of peptidoglycan synthesis inhibitors and suggests additional damage based on an overall disturbance of the membrane topology. In addition, the observed CO release has to be taken into account, which probably also contributes to cell death in a multifarious manner.

Interestingly, Metzler-Nolte and co-workers observed similar pleiotropic antibacterial effects while studying derivatives of the $[Re(CO)_3(dpa\text{-}R)]^+$ type, where the R substituents contain short PNA chains that can be terminated by organometallic moieties such as ferrocene, ruthenocene, or cymanthrene or simply by organic isosteres. Several of these complexes showed antibacterial activity against *S. aureus* in the same range of low micromolar MIC values, as did **ReBpyCtz**. Also, in their case, the dpa-R ligand alone, that is, without the $\{Re(CO)_3\}^+$ fragment, was innocuous, just like other $[Re(CO)_3(dpa\text{-}R')]^+$ complexes, where R′ did not contain the PNA chains. Moreover, the PNA chain-containing fragment was also devoid of any bactericidal activity. Consistent with our results, only the combined molecular constructions formed by the same fragment *fac*-$\{Re(CO)_3\}d^6$ and linked to particular organic components exhibited bactericidal activity.

The antibacterial potential of **ReBpyCtz** is clearly greater than that of either precursor **ReBpyBr** or Ctz alone, and it is tempting to speculate which component might have contributed which feature to the resulting hybrid. The membrane is the established target site of clotrimazole, and as an antifungal drug, it is used against lanosterole-14-demethylase in fungal ergosterol biosynthesis.[45] With its imidazole portion, Ctz binds to iron in the protoporphyrin ring at the active site of the enzyme, and with its remaining part, it interacts with the apo-enzyme. Activities against further membrane-standing enzymes and ion channels have also been reported in mammalian cells.[45] Apart from directly interfering with membrane enzymes, clotrimazole was shown to bind to lipids, and particularly, the addition of unsaturated phospholipids effectively antagonized its antimycotic activity against *C. albicans*.[46] The effects that we observed in our current study for bacterial membranes are consistent with these previous results. We here report undecaprenyl-pyrophosphate and to a lesser degree lipid II as additional lipid species that can be bound by Ctz. While Ctz demonstrated the highest affinity for undecaprenyl-pyrophosphate among the peptidoglycan precursors tested, **ReBpyCtz** showed binding preference for lipid II, which contains a larger head group. The second component, **ReBpyBr**, may bestow additional interaction sites to the hybrid, enhancing the affinity for the carbohydrate portion of lipid I and II and allowing for stronger peptidoglycan synthesis inhibition.

In conclusion, our results clearly demonstrate the enhanced antibacterial activity of **ReBpyCtz** compared to that of free clotrimazole and shed light on the MoA of this kind of conjugated CORMs. It involves a sequence of events initiated by fast and efficient membrane insertion that is most probably followed by a pleiotropic mechanism of bacterial growth inhibition. The cytoplasmic membrane is disorganized, peptidoglycan synthesis is blocked, CO is released, and the membrane potential breaks down. The overall outcome is the killing of the pathogens at a much lower concentration than that with clotrimazole alone. Thus, the promoter effect of these $[M(CO)_3(L{-}L)]^+$ (M = Mn and Re) fragments can be potentially exploited to increase the activity of other antibiotics, contributing to overcome the developed antibiotic resistance shown by several human pathogens.

MATERIALS AND METHODS

Synthesis of CORMs

All manipulations were carried out under a dry nitrogen atmosphere using standard Schlenk techniques. Solvents for reactions and column chromatography were degassed and distilled from the indicated drying agents (in brackets): tetrahydrofuran, abbrv. THF (Na), diethyl ether (Na), methanol (Na), dichloromethane (CaH_2), hexane (CaH_2), and ethyl acetate (Na_2SO_4). Acetone was dried over 4 Å molecular sieves under a nitrogen atmosphere, and water was degassed. $Mn(CO)_5Br$ and $Re(CO)_5Br$ were acquired from Strem Chemicals (Europe). 2,2′-Bipyridyl (Bpy), 2,2′-biquinoline (Biq), 2-pyridyl-benzimidazole, pyridyl-imidazole-2-ylidene ($PyNHC^{Me}$), 4,4′-dinonyl-2,2′-bipyridyl (Bpydinon), and clotrimazole (Ctz) were acquired from Sigma-Aldrich, and $Ag(CF_3SO_3)$ was acquired from Alfa Aesar. Literature methods were used to prepare the following complexes: $Mn(CO)_3Br(Bpy)$,[47] $Re(CO)_5Br$,[48] $Re(CO)_3Br(Bpy)$,[49] *fac*-$[Mn(CO)_3(Biq)Br]$,[21] *fac*-$[Mn(CO)_3(2\text{-pyridyl-benzimidazo-le})Br]$,[50] $Mn(PyNHC^{Me})(CO)_3Br$,[51] and $Mn(BisNHC^{Me})(CO)_3Br$, in which $BisNHC^{Me}$ is bis-imidazole-2-ylidene.[22] The purity of the compounds used in the biological tests was established as ≥95% via C, H, N, and S elemental analyses performed by the Elementary Analysis service of Instituto de Tecnologia Química e Biológica António Xavier, Universidade Nova de Lisboa, Oeiras, Portugal, using a LECO TruSpec CHN Micro elemental analyzer.

Complex **MnBpyCtz** was prepared with triflate instead of PF_6^- as the counterion using a slightly modified previously published protocol,[16] and the FTIR, NMR, and elemental analyses were in agreement with the earlier data.

https://doi.org/10.1021/acsbiomedchemau.2c00007
ACS Bio Med Chem Au 2022, 2, 419−436

NMR spectra were recorded on a Bruker AVANCE III 400 spectrometer. Chemical shifts are quoted in parts per million (ppm) from the residual protic solvent signal (acetone-d_6: ^{1}H 2.05 ppm; CD_2Cl_2: ^{1}H 5.32 ppm; and DMSO-d_6: ^{1}H 2.50 ppm and ^{13}C 39.52 ppm), and coupling constants J are given in Hertz.

FTIR spectra (KBr pellets or ATR) were recorded in an Unicam Mattson 7000 spectrophotometer. Intensities of the stretching vibrations are marked as very strong (vs), strong (s), medium (m), and weak (w). HRMS−electrospray ionization MS (ESI-MS) mass spectra were recorded using a Micromass Quatro LC instrument; nitrogen was employed as a drying and nebulizing gas. The synthesis of the several compounds was pefrormed as follows.

1-*fac*-[$Mn(CO)_3$(Bpy)Ctz][OTf]: to an orange solution of Mn-$(CO)_3$(Bpy)Br (150 mg; 0.4 mmol) in acetone (12 mL) was added $Ag(CF_3SO_3)$ (123 mg; 0.48 mmol), and the solution was left stirring at room temperature for 3 h in the dark. The yellow solution was filtered to discard AgBr, followed by the addition of Ctz (166 mg; 0.48 mmol), and the suspension was left stirring overnight at room temperature. The solution was then evaporated to dryness, and the residue was washed with diethyl ether. A yellow powder was isolated by filtration after recrystallization from CH_2Cl_2/diethyl ether (1:8) at −20 °C for 48 h and dried (250 mg, 79%). Anal. Calcd (%) for $C_{36}H_{25}ClF_3MnN_4O_6S$, (789.1): C, 54.8; H, 3.19; N, 7.10; S, 4.06. Found: C, 54.8; H, 3.25; N, 6.89; S, 4.26. FTIR (KBr; νCO; cm^{-1}): 1941 (vs), 2038 (vs). ^{1}H NMR (400 MHz, DMSO-d_6, 25 °C): δ (ppm) 9.22 (d, J = 5.0 Hz, 2H), 8.59 (d, J = 8.0 Hz, 2H), 8.26 (td, J = 8.0, 1.3 Hz, 2H), 7.73−7.69 (m, 2H), 7.46 (td, J = 7.9, 1.4 Hz, 1H), 7.40−7.31 (m, 8H), 6.98 (dt, J = 12.3, 1.4 Hz, 2H), 6.72 (d, J = 6.9 Hz, 4H), 6.68 (dd, J = 7.9, 1.4 Hz, 1H), 6.53 (s, 1H).

2-*fac*-[$Re(CO)_3$(Bpy)Ctz][OTf]: to a greenish solution of Re-$(CO)_3$(Bpy)Br (202 mg; 0.4 mmol) in acetone (30 mL), $Ag(CF_3SO_3)$ (123 mg; 0.48 mmol) was added, and the solution was left stirring at room temperature for 3 h in the dark. The solution was filtered to discard AgBr, and after the addition of Ctz (166 mg; 0.48 mmol), the suspension was left stirring overnight at room temperature. The solution was then evaporated to dryness, and the solid was washed with diethyl ether. A yellow powder was isolated by filtration after recrystallization from CH_2Cl_2/diethyl ether (1:8) at −20 °C for 5 days and dried (239 mg; 65%). Anal. Calcd (%) for $C_{36}H_{25}ClF_3ReN_4O_6S$, (920.3): C, 47.0; H, 2.74; N, 6.09; S, 3.48. Found: C, 46.8; H, 2.72; N, 5.95; S, 3.56. FTIR (KBr; νCO; cm^{-1}): 1914 (vs), 1936 (vs), 2028 (vs). ^{1}H NMR (400 MHz, DMSO-d_6, 25 °C): δ (ppm) 9.12 (d, J = 5.2 Hz, 2H), 8.68 (d, J = 8.1 Hz, 2H), 8.34 (td, J = 8.1, 1.2 Hz, 2H), 7.75−7.72 (m, 2H), 7.47 (td, J = 7.7, 1.2 Hz, 1H), 7.40−7.31 (m, 8H), 7.03 (d, J = 19.1 Hz, 2H), 6.82 (s, 1H), 6.7−6.71 (m, 5H).

3-*fac*-[$Mn(CO)_3$(Biq)Ctz][OTf]: *fac*-[$Mn(CO)_3$(Biq)Br] (124 mg; 0.28 mmol), $Ag(CF_3SO_3)$ (77.3 mg; 0.3 mmol), and Ctz (97.3 mg; 0.28 mmol) were dissolved in acetone (30 mL). The mixture was warmed to 50 °C, stirred overnight, and then dried. The oily residue was mixed in toluene (25 mL) and filtered through a Celite plug to remove AgBr. After the evaporation of toluene, the residue was dissolved in MeOH (10 mL). The solution was covered with a layer of diethyl ether (40 mL) and kept in the dark at 5 °C. Red crystals that were recovered by filtration were washed with ether and dried under high vacuum. Anal. Calcd (%) for: $C_{44}H_{29}N_4ClMnSF_3O_6$, (889.2): C, 59.43; H, 3.29; N, 6.3; S, 3.6. Found: C, 59.24; H, 3.19; N, 5.91; S, 3.99. FTIR (νCO; cm^{-1}): 2031 (s), 1943 (vs). HRMS ESI-MS (positive mode): 739.1304 [M]$^+$; 277.0776 [$Ph_2(C_6H_4Cl)$-C]$^+$. ^{1}H NMR (400 MHz, acetone-d_6, 25 °C): δ (ppm) 8.97 (dd, J = 8.8 Hz, 4H), 8.83 (d, J = 8.6 Hz, 2H), 8.33 (d, J = 8.2 Hz, 2H), 8.26 (t, J = 8.2 Hz, 2H), 8.00 (t, J = 7.4 Hz, 2H), 7.52−7.24 (m, 10H), 6.84 (s, 1H), 6.78 (d, J = 7.6 Hz, 4H), 6.26 (s, 2H).

4-*fac*-[$Mn(CO)_3$(2-pyridyl-benzimidazole)(Ctz)][OTf]: *fac*-[Mn-$(CO)_3$(2-pyridyl-benzimidazole)Br] (151 mg; 0.36 mmol), Ag-(CF_3SO_3) (93.4 mg; 0.36 mmol), and Ctz (126 mg, 0.37 mmol) were dissolved in acetone (30 mL). The mixture was warmed to 50 °C, stirred overnight, and then left to dry. The oily residue was mixed in toluene (25 mL) and filtered through a Celite plug to remove AgBr. After the evaporation of toluene, the resulting yellow-brown foam was ground in hexane at very low temperature (thawing from liquid nitrogen solidification), producing a yellow powder that was separated by decantation and chromatographed in a silica gel column. After elution with dichloromethane, the product was treated with acetone and dried in vacuum to produce a yellow-greenish foam, which was dried under high vacuum. Anal. Calcd (%) for $C_{38}H_{26}N_5ClMnSF_3O_6$, (828.1): C, 55.12; N, 8.46; H, 3.16; S, 3.87. Found: C, 55.31; N, 8.20; H, 3.43; S, 3.95. FTIR (νCO; cm^{-1}): 2024 (s), 1906 (vs). HRMS ESI-MS (positive mode): 678.1090 [M]$^+$; 277.0776 [$Ph_2(C_6H_4Cl)$-C]$^+$. ^{1}H NMR (400 MHz, acetone-d_6, 25 °C): δ (ppm) 9.27 (d, J = 5.3 Hz, 1H), 8.23 (d, J = 6.8 Hz, 1H), 7.91 (t, J = 4.4 Hz, 1H), 7.68 (t, J = 6.0 Hz, 1H), 7.48−7.18 (m, 15H), 6.93 (s, 1H), 6.85 (s, 1H), 6.74 (t, J = 6.9 Hz, 4H), 6.66 (s, 1H), 6.59 (d, J = 7.9 Hz, 1H).

5-*fac*-[$Mn(CO)_3$(4,4′-dinonyl-2,2′-bipyridyl)(Ctz)][OTf]: a solution of $Mn(CO)_5Br$ (275 mg, 1 mmol) magnetically stirred in acetone (40 mL) was treated with $Ag(CF_3SO_3)$ (257 mg, 1 mmol) for 10 min at room temperature in the dark and then refluxed for 1 h to form $[Mn(CO)_3(OCMe_2)_3][CF_3SO_3]$.[52] The precipitate of AgBr was filtered off, and 4-4′-dinonyl-2-2′-bipyridyl (407 mg; 1 mmol) was added, followed by Ctz (345 mg; 1 mmol). The mixture was allowed to react for 1 h at reflux and then concentrated to give an oily residue, which was washed with hexane and dried. The oily residue was chromatographed on an alumina column under nitrogen and eluted with ethyl acetate/CH_2Cl_2. The yellow fraction collected was left to dry, which originated a yellow foam that was dried in vacuum. Anal. Calcd (%) for $C_{54}H_{61}N_4ClF_3O_6MnS$, (1041.5): C, 62.27; H, 5.90; N, 5.38; S, 3.08. Found: C, 61.90; H, 6.15; N, 5.26; S, 3.10. FTIR (νCO; cm^{-1}): 2031 (s), 1929 (vs). ^{1}H NMR (400 MHz, CD_2Cl_2, 25 °C): δ (ppm) 8.92 (d, J = 5.6 Hz, 2H), 8.00 (s, 2H), 7.41−7.25 (m, 12H), 6.82 (d, J = 7.5 Hz, 4H), 6.72 (s, 1H), 6.67 (d, J = 6.4 Hz, 2H), 2.81 (t, J = 7.4 Hz, 4H), 1.69 (m, J = 6.3 Hz, 4H), 1.38 (s, 4H), 1.29 (s, 20H), 0.88 (t, J = 6.7 Hz, 6H).

6-*fac*-[Mn(*N*-methyl-*N*′-2-pyridylimidazol-2-ylidene)$(CO)_3$Ctz]-[OTf]: silver triflate (135 mg, 0.5 mmol) was added to a solution of $Mn(PyNHC^{Me})(CO)_3Br$ (200 mg; 0.47 mmol) in degassed acetone (15 mL), and the mixture was stirred in the dark for 3 h. The solution was filtered under a nitrogen atmosphere, and Ctz (181 mg; 0.53 mmol) was added to the filtrate. After stirring the mixture in the dark for 20 h, the solvent was removed, and the residue was recrystallized from CH_2Cl_2/diethyl ether. The resulting precipitate was collected and washed with ether to afford the product as a pale solid. Yield: 104 mg, 23%. Anal. Calcd (%) for $C_{35}H_{26}MnN_5O_6ClF_3S$, (792.1): C, 53.07; H, 3.31; N, 8.84; S, 4.05. Found: C, 52.70; H, 3.19; N, 9.12; S, 3.99. FTIR (KBr, νCO; cm^{-1}): 2030 (s), 1941 (s), 1919 (s). HRMS ESI-MS-(positive mode): 642.1098 [M]$^+$. ^{1}H NMR (400 MHz, DMSO-d_6, 25 °C): δ (ppm) 8.41 (s, 1H), 8.24 (t, J = 7.7 Hz, 1H), 8.08 (d, J = 8.4 Hz, 1H), 7.72 (s, 1H), 7.50−7.42 (m, 3H), 7.38−7.33 (m, 7H), 6.98 (s, 1H), 6.89 (s, 1H), 6.79 (t, J = 6.1 Hz, 4H), 6.72 (d, J = 7.9 Hz, 1H), 6.58 (s, 1H), 4.02 (s, 3H). ^{13}C NMR (DMSO-d_6, 25 °C): δ (ppm) 223.20 (CO), 217.95 (CO), 214.93 (CO), 197.88 (Mn-$C_{carbene}$), 153.58, 152.10, 142.51, 140.53, 139.44, 139.17, 138.02, 134.32, 132.32, 131.35, 131.05, 130.82, 129.22, 129.10, 128.62, 128.44, 127.72, 127.45, 124.11, 123.62, 117.67, 112.53, 75.64 (NCH_2N), 37.81 (NCH_3).

7-*fac*-[Mn(methylene bis-*N*-methylimidazole-2-ylidene)-$(CO)_3$(Ctz)][OTf]: silver triflate (91 mg; 0.35 mmol) was added to a solution of $Mn(BisNHC^{Me})(CO)_3Br$ (117 mg; 0.29 mmol) in degassed acetone (10 mL), and the mixture was stirred in the dark for 3 h. The solution was filtered under a nitrogen atmosphere, and Ctz (122 mg; 0.35 mmol) was added to the filtrate. After stirring in the dark for 20 h, the solvent was removed, and the residue was recrystallized via diffusion with CH_2Cl_2/diethyl ether. The resulting precipitate was collected and dried under vacuum to obtain the product as a pale solid. Anal. Calcd (%) for $C_{35}H_{29}MnN_6O_6ClF_3S.0.2CH_2Cl_2$, (809.1): C, 51.18; H, 3.59; N, 10.17; S, 3.88. Found: C, 50.69; H, 3.41; N, 10.25; S, 4.41. FTIR (KBr, νCO; cm^{-1}): 2013 (s), 1927 (s), 1899 (s). HRMS ESI-MS-(positive mode): 659.1362 [M]$^+$. ^{1}H NMR (400 MHz, DMSO-d_6, 25 °C): δ (ppm) 7.58 (d, J = 1.5 Hz, 2H), 7.53−7.49 (m, 2H), 7.44 (d, J = 1.5 Hz, 3H), 7.41−7.36 (m, 6H), 7.11 (s, 1H), 6.95−6.89 (m, 5H),

https://doi.org/10.1021/acsbiomedchemau.2c00007
ACS Bio Med Chem Au 2022, 2, 419−436

6.09−5.91 (m, 2H), 5,76 (s, 1H), 3.89 (s, 1H), 3.48 (s, 6H) ^{13}C NMR (DMSO-d_6, 25 °C): δ (ppm) 220.74 (*CO*), 218.35 (*CO*), 188.73 (Mn-$C_{carbene}$), 141.79, 139.23, 138.29, 133.99, 132.40, 131.00, 130.53, 128.91, 128.42, 127.75, 124.29, 123.66, 122.13, 75.60 (NCH_2N), 36.96 (NCH_3). Note: it was not possible to completely remove crystallization CH_2Cl_2 and improve the purity of the crystalline compound.

Bacterial Strains

The bacterial strains used in this work were *E. coli* K12 MG1655; *S. enterica* serovar Typhimurium SL1344; *S. aureus* USA300 JE2 (MRSA) (NARSA, Chantilly, VA, United States); *S. aureus* NCTC8325; *S. aureus* ATCC29213; *B. subtilis* 1S34; *B. subtilis* 168 strain TMB1617; *E. faecium* BM4147-1; *Klebsiella pneumoniae* ATCC12657; *Enterobacter aerogenes* ATCC13048; *P. aeruginosa* ATCC27853; and *Acinetobacter baumannii* 09987.

Growth Rate Determination

Overnight cultures were used to inoculate fresh media to an optical density at 600 nm (OD_{600nm}) of 0.1. When cells reached an OD_{600nm} of 0.3, they were treated with the compounds or with 1% (v/v) of the respective solvent. The growth rates were determined at up to 24 h for at least three biological samples. Unpaired *t*-test was performed for each condition using GraphPad Prism version 7.0 for iOS, GraphPad Software, La Jolla California USA.

MIC Determination

The MIC values represented in Table 1 were determined using the broth microdilution method in cation-adjusted Mueller−Hinton broth according to the guidelines of the Clinical and Laboratory Standards Institute (CLSI), as previously described.[53] Briefly, a 2-fold serial dilution of the compound (starting from 32 μg/mL) was prepared in polystyrene microtiter plates and seeded with a final bacterial inoculum of 5×10^5 colony-forming units (cfu) per mL. After overnight incubation at 37 °C, while shaking at 90 rpm, in ambient air, the lowest compound concentration preventing visible bacterial growth was considered the MIC. For the values presented in Table S2, the microtiter plates were inoculated with an overnight culture of *E. coli*, *S. aureus*, and *S. enterica* with approximately 10^7 cfu/mL and incubated for 18 h at 37 °C while shaking at 90 rpm. MIC values were determined in triplicate for at least three independent experiments.

Mammalian Cell Cytotoxicity Assay

The porcine kidney epithelial cell line (LLC-PK1) was grown in Dulbecco's modified Eagle's medium (DMEM) supplemented with 10% (v/v) heat-inactivated foetal bovine serum (FBS) and a 1% (v/v) penicillin−streptomycin mixture. The human hepatoma cell line (HepG2) was cultured in Eagle's minimum essential medium supplemented as described above. Cells were distributed into 96-well plates at a density of 10,000 cells/well. The plates were incubated for 24 h for cell seeding. On the second day, the compounds were administered, and three independent biological samples were tested in triplicate. After 24 h, the culture medium was discarded, and 100 μL of fresh medium containing 0.5 mg/mL MTT, preheated at 37 °C, was added to each well. The cells were then incubated in the dark for 1 h at 37 °C, in a 5% CO_2 atmosphere. After the removal of the medium, the formazan crystals were solubilized with 100 μL of DMSO. The absorbance was measured spectrophotometrically at 550 nm in a Multiskan GO microplate spectrophotometer, Thermo Scientific. The IC_{50} value was calculated using software Prism 5 (GraphPad) by fitting the best dose−response curve to the normalized data set.

In Vitro CO Release in Blood and Bacteria

CORM solutions were prepared in DMSO, and 50 μL of the solution swas added to 1 mL of sheep whole blood in Alsever's solution (TCS Biosciences Ltd, UK) and incubated at 37 °C. A final concentration of 0.3 mg mL^{-1} of CORM was used to mimic an *in vivo* dosage of approximately 25 mg kg^{-1} for an average 20 g mouse. To follow the increase of the CO−hemoglobin (COHb) levels, samples were analyzed over time in an Avoximeter 4000 from A-vox Instruments Inc. The released CO was calculated based on the amount of the compound initially added, the total amount of hemoglobin used, and the %COHb formed. Control spectra of untreated blood samples were recorded. The experiment was performed with two different blood batches.

Determination of the CO released from CORMs into bacteria was carried out using carbon monoxide probe-1, COP-1, as previously described.[54] Briefly, bacterial cells grown aerobically in LB to an OD_{600} of ∼0.3 were incubated with the selected CORMs for 15 min at 37 °C and 150 rpm. Bacteria were incubated with 1 μM COP-1 for 15 min, after which an aliquot was obtained, washed with phosphate-buffered saline (PBS), and analyzed in a Leica DM6000B fluorescence microscope, with a phase contrast Uplan F1 100× objective and a CCD Ixon camera (Andor Technologies). All samples were excited at 488 nm with filter set for fluorescein isothiocyanate, and the emission was collected using a META detector at 525 nm. The microscope images were analyzed using ImageJ software version 2.3.0/1.53f. Images were captured from at least three biological samples, and in total, at least 300 cells were analyzed.

Bioreporter Assays

For target pathway detection, induction of the firefly luciferase linked to the promoters of *yorB*, *helD*, *yheI*, *ypuA*, or *liaI* in the genetic background of *B. subtilis* 1S34 was determined as previously described.[55] Reporter signals were recorded in either Belitzky minimal medium (BMM) (*yheI* strain) or LB medium (all other strains). Serial 2-fold dilutions of the test compounds (starting at 4× MIC for Ctz and **ReBpyCtz** and at 64 μg/mL for ReBpyBr) in 60 μL of LB or BMM were prepared in white 96-well flat-bottom polystyrene microtiter plates, and plates were inoculated with 60 μL of a bacterial suspension adjusted to an OD_{600nm} of 0.02. Plates were incubated at 37 °C for a predetermined time depending on the induction kinetics of the reporter strain: 1 h for the *liaI* and *ypuA* reporters, 1.5 h for the *helD* strain, 3.5 h for the *yorB* strain, and 4 h for the *yheI* strain. Then, 60 μL of citrate buffer (0.1 M, pH 5) containing 2 mM luciferin (Serva) was added, and flash luminescence was recorded using a microtiter plate reader (TECAN infinite M200).

For the bioreporter quenching assay with purified peptidoglycan precursors, *B. subtilis* 168 strain TMB1617 was employed, in which the *liaI* promotor was fused to the bacterial luciferase from *P. luminescens* (P_{lia}-lux),[56] and the assay was conducted as described previously.[57] The bioreporter was grown to an OD_{600nm} of 0.5 at 30 °C in cation-adjusted Mueller−Hinton broth containing 5 μg/mL chloramphenicol and added to microtiter plates containing 2-fold dilution series of **ReBpyCtz**, ReBpyBr, or Ctz. Luminescence was measured every 15 min for 10 h at 30 °C using a Spark 10M microplate reader (Tecan). Purified cell wall precursors lipid II, C_{55}PP, or C_{55}P were tested for their ability to antagonize the stress response. The peptidoglycan precursors were added in a 10-fold molar excess over the test compounds and preincubated with the compounds for 15 min, before the cells were added, and luminescence was measured as described above.

Membrane Labeling in Live Cell Microscopy

FM 5-95 labeling after antibiotic exposure was conducted as described.[58] Briefly, *S. aureus* NCTC8325 was grown in LB medium at 37 °C and 200 rpm to an OD_{600} of 0.3. Culture aliquots were treated with either Ctz (8 μg/mL, 2× MIC), ReBpyBr (64 μg/mL), or **ReBpyCtz** (0.5 μg/mL, 2× MIC), using DMSO (1%) as a negative control, and incubated at 37 °C for 30 min. Samples were labeled with 20 μg/mL *N*-(3-trimethylammoniumpropyl)-4-(6-(4-(diethylamino)-phenyl)hexatrienyl) pyridinium dibromide (FM 5-95, Molecular Probes) and visualized via fluorescence microscopy (λ_{Ex} 506 nm and a window for emission from 650 to 700 nm) on microscope slides covered with a thin film of 1% agarose using a Nikon Eclipse Ti-E microscope. Images were acquired on an Orca Flash 4.0 LT camera (Hamamatsu) using software NIS Elements Advanced Research (Nikon) and further analyzed and processed using software NIS Elements.

https://doi.org/10.1021/acsbiomedchemau.2c00007
ACS Bio Med Chem Au 2022, 2, 419−436

Microscopic Cell Wall Integrity Assay and HADA Incorporation Microscopy

B. subtilis 168 was grown in cation-adjusted Mueller−Hinton medium at 37 °C and 200 rpm to an OD_{600} of 0.35. Aliquots (100 μL) of the cells were treated with Ctz (8 μg/mL, 4× MIC), **ReBpyCtz** (1 μg/mL, 4× MIC), and ReBpyBr (64 μg/mL). Vancomycin (2 μg/mL, 8× MIC) and DMSO (1%) served as positive and negative controls, respectively. After 30 min incubation, 25 μL of cells was transferred to a fresh tube containing 100 μL of a 1:3 (v/v) mixture of acetic acid and methanol. Samples were imaged using brightfield microscopy on microscope slides covered with a thin film of 1% agarose using a Zeiss Axio Observer Z1 automated microscope. Images were acquired using an Orca Flash 4.0 V2 camera (Hamamatsu) and an alpha Plan-Apochromat 100×/1.46 Oil Ph3 objective (Zeiss). Images were processed using the Zen software package (Zeiss).

To monitor the effect of CORMs on peptidoglycan synthesis microscopically, we stained *B. subtilis* cells with the fluorescent D-amino-acid HCC-amino-D-alanine (HADA) probe,[59] which was custom-synthesized by EMC Microcollections (Tübingen). Cells were grown in LB overnight at 37 °C and 180 rpm, diluted 1:100 in fresh medium, and grown at 37 °C to an OD_{600} of 0.3−0.4. Aliquots of 500 μL in 24-well plates were treated for 5 min at 37 °C and 500 rpm with Ctz (4 μg/mL, 2× MIC), **ReBpyCtz** (0.5 μg/mL, 2× MIC and 1 μg/mL, 4× MIC), ReBpyBr (64 μg/mL), or carbonyl cyanide 3-chlorophenylhydrazone (CCCP, 5 μM). DMSO (0.5%) served as a negative control. Then, samples were centrifuged (5000*g*, 5 min), most of the supernatant (450 μL) was removed, and cells were labeled in the remaining 50 μL with a final concentration of 1 mM HADA and mixed briefly by vortexing and incubation for 3.5 min at 37 °C. The reaction was stopped by adding 1 mL of ice-cold PBS, and unbound dye was removed via three washing steps with ice-cold PBS (16,000 rpm, 3 min, 4 °C). Subsequently, the cells were placed on microscopy slides covered with a thin layer of agarose (1.2% in PBS) and visualized via brightfield and fluorescence microscopy in a Zeiss Axio Observer Z1 LSM800 at a λ_{ex} of 353 nm and a λ_{em} of 465 nm. Images were acquired using an Orca Flash 4.0 V2 camera (Hamamatsu) and an α Plan-Apo 100×/1.46 Oil Ph3 objective (Zeiss). To quantitatively assess D-amino-acid incorporation, all samples were stained and imaged under the same conditions. Image processing was performed in FIJI,[60] and the relative fluorescence units of the HADA signals in the septal regions were quantified using MicrobeJ.[61] Cells were identified in the phase contrast channel with a width limit from 0.5 to 1.3 μm and a length above 2 μm. Lysed cells, if present, were excluded from the analysis. The septal HADA labeling intensity was then quantified within individual cells ($N > 100$), and the data were further analyzed and plotted using GraphPad Prism software. The significance was determined via one-way ANOVA.

Membrane Potential Measurement and Membrane Pore Formation

The membrane potential of *S. aureus* NCTC8325 was determined as described previously.[62] Briefly, cells grown in LB were resuspended in PBS, loaded with 3,3′-diethyloxacarbocyanine iodide [$DiOC_2(3)$, Molecular Probes, Fisher Scientific], and transferred to a black 96-well flat-bottom polystyrene microtiter plate. Baseline measurements were obtained in a microplate reader (TECAN Spark) for 2 min [λ_{ex} = 485 nm; and two emission wavelengths λ_{em} = 530 nm (green) and λ_{em} = 630 nm (red)], after which Ctz, ReBpyBr, and **ReBpyCtz** were added in concentration series, and the measurement was continued as above for a total of 15 min. CCCP (5 μM) was used as a positive control and DMSO (1%) as a negative control.

Pore formation was monitored as described[62] using the Live/Dead BacLight bacterial viability kit (Molecular Probes). *S. aureus* NCTC8325 was grown in LB and treated for 120 min with either Ctz (16 μg/mL, 4× MIC), ReBpyBr (64 μg/mL), **ReBpyCtz** (1 μg/mL, 4× MIC), a crude preparation of the pore-forming antibiotic nisin (100 μg/mL, Sigma-Aldrich, positive control), or DMSO (1%, negative control). Then, cells were labeled with a mixture of syto9 and PI for 15 min and visualized via brightfield and fluorescence microscopy in a Zeiss Axio Observer Z1 automated microscope at λ_{ex} 483 nm/λ_{em} 500 nm emission (syto9) and λ_{ex} 305 nm/λ_{em} 617 nm emission (PI) on agarose-covered microscope slides. Images were acquired using an Orca Flash 4.0 V2 camera (Hamamatsu) and an alpha Plan-Apochromat 100×/1.46 Oil Ph3 objective (Zeiss) and processed using the Zen software package (Zeiss).

Quantification of UDP-MurNAc-PP

Metabolite extraction was performed as described.[63] Briefly, *S. aureus* ATCC29213 was grown in LB medium at 37 °C and 200 rpm to an OD_{600} of 0.5; then, 130 μg/mL of chloramphenicol was added; and incubation was continued for further 15 min. Aliquots of 5 mL were treated with **ReBpyCtz**, ReBpyBr, Ctz, or vancomycin as the positive control for 30 min at the indicated concentrations. Cells were cooled on ice, washed with Millipore water, pelleted, and frozen. For analysis, pellets were resuspended in 500 μL of Millipore water and disrupted in a Precellys Evolution homogenizer at 3 × 20 s, 6500 rpm with 30 s intervals using 0.1 mm glass beads. After centrifugation at 14,000 rpm, 4 °C for 20 min, 400 μL of the supernatant was transferred to a fresh tube containing 1.6 mL of acetone [high-performance liquid chromatography (HPLC) grade]. Samples were centrifuged as above for 15 min, and the supernatant was transferred into a fresh tube and dried in a vacuum centrifuge. Dried samples were resuspended in 50 μL of Millipore water, and 5 μL aliquots were analyzed via LC−MS using a Gemini C18 column (150 × 4.6 mm, 110 Å, 5 mm; Phenomenex) and an UltiMate 3000 RS (Dionex) coupled to a micro-TOF II mass spectrometer (Bruker Daltronics) operated in the negative or positive ionization mode, as indicated. Samples were separated using a 30-min gradient of 0−40% acetonitrile at a flow rate of 0.2 mL/min, as described previously.[64] Extracted ion chromatograms (EICs) were used to calculate the area under the curve (AUC) using Prism 8.4 (GraphPad).

Purification of Cell Wall Precursors

Peptidoglycan precursors lipid I and lipid II were synthesized in a large scale as previously described.[65] Concentrations of purified precursors were determined based on their phosphate content, which was measured *via* a phosphate test according to Rouser *et al.*[66] Uridine diphosphate-*N*-acetyl glucosamine (UDP-MurNAc-PP) used for precursor synthesis was purified in a crude preparation according to the method of Kohlrausch and Höltje.[67] Undecaprenyl phosphate ($C_{55}P$) and undecaprenyl pyrophosphate were purchased from Larodan Fine Chemicals AB (Malmö, Sweden).

In Vitro Lipid II Synthesis with Isolated Bacterial Membranes

Membranes of *M. luteus* were used to determine the inhibitory activity of the compounds for lipid II synthesis by a crude membrane fraction as described previously.[68,69] 5 nmol $C_{55}P$ was used in a total volume of 50 μL containing 0.6% triton X-100, 10 mM $MgCl_2$, 1 mM uridine diphosphate-*N*-acetyl glucosamine (UDP-GlcNAc), and 100 mM Tris−HCl, pH 7.5. **ReBpyCtz**, Ctz, or ReBpyBr was added to lipid carrier $C_{55}P$ in a molar ratio of 10:1 and incubated for 15 min at room temperature. Crude preparations of *Staphylococcus simulans* 22 containing UDP-MurNAc-PP, as well as membrane preparations of *M. luteus,* were added to start the reaction. Samples were incubated at 30 °C for 2 h, extracted with an equal volume of *n*-butanol:pyridine acetate, pH 4.2 (2:1, v/v), and centrifuged for 3 min at 13,500 rpm. The upper phase was applied to thin-layer chromatography (TLC) silica plates and developed in a solvent containing chloroform/methanol/water/ammonia (88:48:10:1, v/v/v/v). Lipid bands were visualized via phosphomolybdic acid staining.[65]

In Vitro Peptidoglycan Biosynthesis with Purified Precursors and Recombinant Purified Enzymes

Synthesis of lipid I and lipid II catalyzed by MraY and MurG, respectively, were performed using purified recombinant enzymes as described previously.[57,70] Briefly, for lipid I synthesis by purified MraY, samples were prepared in a total volume of 50 μL containing 5 nmol substrate $C_{55}P$, 60 mM $MgCl_2$, 1.25 mM $CaCl_2$, 0.6% triton X-100, and 100 mM Tris−HCl, pH 7.5. Reactions were initiated by the addition of a crude extract containing UDP-MurNAc-PP and the

https://doi.org/10.1021/acsbiomedchemau.2c00007
ACS Bio Med Chem Au 2022, 2, 419−436

purified MraY enzyme. After incubation at 30 °C for 2 h, reaction mixtures were extracted as mentioned above and analyzed *via* TLc. MurG-catalyzed lipid II synthesis was conducted using 2 nmol purified lipid I in a final volume of 30 μL that contained 25 nmol UDP-GlcNAc, 0.8% triton X-100, 5.7 mM $MgCl_2$, and 200 mM Tris−HCl, pH 7.5. Samples were incubated at 30 °C for 1 h, extracted, and analyzed *via* TLC, as described above. In all *in vitro* reactions, **ReBpyCtz**, Ctz, and ReBpyBr were added to the purified cell wall precursors in a molar ratio of 10:1 and incubated for 15 min at room temperature, and reactions were started by adding the purified proteins.

■ ASSOCIATED CONTENT

Supporting Information

The Supporting Information is available free of charge at https://pubs.acs.org/doi/10.1021/acsbiomedchemau.2c00007.

FTIR data and 1H NMR spectra for Ctz conjugates; additional experiments on cell viability, membrane depolarization, and integrity; bioreporter profiling; and lipid I biosynthesis (PDF)

■ AUTHOR INFORMATION

Corresponding Authors

Heike Brötz-Oesterhelt − *Interfaculty Institute of Microbiology and Infection Medicine, Dept. of Microbial Bioactive Compounds, Cluster of Excellence Controlling Microbes to Fight Infection, University of Tuebingen, 72070 Tuebingen, Germany;* orcid.org/0000-0001-9364-1832; Email: heike.broetz-oesterhelt@uni-tuebingen.de

Carlos C. Romão − *Instituto de Tecnologia Química e Biológica António Xavier, Universidade Nova de Lisboa, 2780-157 Oeiras, Portugal*; Phone: +351 21 4469328; Email: ccr@itqb.unl.pt

Lígia M. Saraiva − *Instituto de Tecnologia Química e Biológica António Xavier, Universidade Nova de Lisboa, 2780-157 Oeiras, Portugal;* orcid.org/0000-0002-0675-129X; Email: lst@itqb.unl.pt

Authors

Sofia S. Mendes − *Instituto de Tecnologia Química e Biológica António Xavier, Universidade Nova de Lisboa, 2780-157 Oeiras, Portugal*

Joana Marques − *Instituto de Tecnologia Química e Biológica António Xavier, Universidade Nova de Lisboa, 2780-157 Oeiras, Portugal;* orcid.org/0000-0002-7333-9158

Edit Mesterházy − *Instituto de Tecnologia Química e Biológica António Xavier, Universidade Nova de Lisboa, 2780-157 Oeiras, Portugal*

Jan Straetener − *Interfaculty Institute of Microbiology and Infection Medicine, Dept. of Microbial Bioactive Compounds, Cluster of Excellence Controlling Microbes to Fight Infection, University of Tuebingen, 72070 Tuebingen, Germany*

Melina Arts − *Institute for Pharmaceutical Microbiology, University of Bonn, University Clinic Bonn, 53115 Bonn, Germany;* orcid.org/0000-0003-0344-6107

Teresa Pissarro − *Instituto de Tecnologia Química e Biológica António Xavier, Universidade Nova de Lisboa, 2780-157 Oeiras, Portugal*

Jorgina Reginold − *Instituto de Tecnologia Química e Biológica António Xavier, Universidade Nova de Lisboa, 2780-157 Oeiras, Portugal*

Anne Berscheid − *Interfaculty Institute of Microbiology and Infection Medicine, Dept. of Microbial Bioactive Compounds, Cluster of Excellence Controlling Microbes to Fight Infection, University of Tuebingen, 72070 Tuebingen, Germany;* orcid.org/0000-0003-1585-8715

Jan Bornikoel − *Interfaculty Institute of Microbiology and Infection Medicine, Dept. of Microbial Bioactive Compounds, Cluster of Excellence Controlling Microbes to Fight Infection, University of Tuebingen, 72070 Tuebingen, Germany*

Robert M. Kluj − *Institute of Microbiology and Infection Medicine, Dept. of Organismic Interactions, University of Tuebingen, 72070 Tuebingen, Germany*

Christoph Mayer − *Institute of Microbiology and Infection Medicine, Dept. of Organismic Interactions, University of Tuebingen, 72070 Tuebingen, Germany;* orcid.org/0000-0003-4731-4851

Filipp Oesterhelt − *Interfaculty Institute of Microbiology and Infection Medicine, Dept. of Microbial Bioactive Compounds, Cluster of Excellence Controlling Microbes to Fight Infection, University of Tuebingen, 72070 Tuebingen, Germany*

Sofia Friães − *Instituto de Tecnologia Química e Biológica António Xavier, Universidade Nova de Lisboa, 2780-157 Oeiras, Portugal*

Beatriz Royo − *Instituto de Tecnologia Química e Biológica António Xavier, Universidade Nova de Lisboa, 2780-157 Oeiras, Portugal;* orcid.org/0000-0002-7909-9992

Tanja Schneider − *Institute for Pharmaceutical Microbiology, University of Bonn, University Clinic Bonn, 53115 Bonn, Germany*

Complete contact information is available at: https://pubs.acs.org/10.1021/acsbiomedchemau.2c00007

Author Contributions

The manuscript was written through contributions of all authors.

Funding

This work was financially supported by Fundação para a Ciência e Tecnologia (Portugal) through fellowship PD/BD/148006/2019 (SSM), PTDC/SAU-INF/29313/2017 grant, and R&D unit LISBOA-01-0145-FEDER007660 (MostMicro) cofounded by FCT/MCTES and FEDER funds under the PT2020 Partnership Agreement. The NMR data was acquired at CERMAX, Instituto de Tecnologia Química e Biológica António Xavier, Universidade Nova de Lisboa, Oeiras, Portugal, with equipment funded by FCT, project AAC 01/SAICT/2016. This work was partially supported by the PPBI—Portuguese Platform of BioImaging (PPBI-POCI-01-0145-FEDER-022122) cofunded by national funds from OE—"Orçamento de Estado" and by European funds from FEDER—"Fundo Europeu de Desenvolvimento Regional". LMS and SSM acknowledge funding from the European Union's Horizon 2020 research and innovation program under grant agreement no. 810856. H.B.-O., T.S., C.M., F.O., J.B., and M.A. gratefully acknowledge funding by the Deutsche Forschungsgemeinschaft (DFG, German Research Foundation), project ID 398967434 (TRR 261, projects A01, A06, A10, and Z02). A.B. appreciates funding by the German Federal Ministry for Education and Research (project Gram-neg. Design).

Notes

The authors declare no competing financial interest.

ABBREVIATIONS

$BisNHC^{Me}$	methylene bis(*N*-methylimidazolylidene)
Bpy	2,2′-bipyridyl
Bpydinon	4,4′-dinonyl-2,2′-bipyridyl
Biq	2,2′-biquinoline
CO	carbon monoxide
CORM	carbon monoxide-releasing molecule
DMEM	Dulbecco's modified Eagle's medium
Dpa	di-(2-picolyl)amine
FBS	heat-inactivated fetal bovine serum
FI	fluorescence intensity
HADA	HCC-amino-D-alanine
MIC	minimal inhibitory concentration
MS	minimal salt medium
MRSA	methicillin-resistant *Staphylococcus aureus*
PBS	phosphate-buffered saline
PyBzim	2-pyridyl-benzimidazole
$PyNHC^{M}e$	*N*-methyl-*N*′-2-pyridylimidazolium
Tpa	tris(2-pyridylmethyl)amine
UDP-GlcNAc	uridine diphosphate-*N*-acetyl glucosamine
UDP-MurNAc-PP	UDP-*N*-acetylmuramic acid-pentapeptide
lipid I	undecaprenyl-pyrophosphoryl-MurNAc-pentapeptide
lipid II	UDP-*N*-acetylmuramic acid-pentapeptide-*N*-acetyl glucosamine

REFERENCES

(1) Motterlini, R.; Otterbein, L. E. The Therapeutic Potential of Carbon Monoxide. *Nat. Rev. Drug Discovery* **2010**, *9*, 728−743.

(2) Nobre, L. S.; Seixas, J. D.; Romão, C. C.; Saraiva, L. M. Antimicrobial Action of Carbon Monoxide-Releasing Compounds. *Antimicrob. Agents Chemother.* **2007**, *51*, 4303−4307.

(3) Mendes, S. S.; Miranda, V.; Saraiva, L. M. Hydrogen Sulfide and Carbon Monoxide Tolerance in Bacteria. *Antioxidants* **2021**, *10*, 729−746.

(4) Wareham, L. K.; Poole, R. K.; Tinajero-Trejo, M. CO-Releasing Metal Carbonyl Compounds as Antimicrobial Agents in the Post-Antibiotic Era. *J. Biol. Chem.* **2015**, *290*, 18999−19007.

(5) Johnson, T. R.; Mann, B. E.; Teasdale, I. P.; Adams, H.; Foresti, R.; Green, C. J.; Motterlini, R. Metal Carbonyls as Pharmaceuticals? [Ru(CO)3Cl(Glycinate)], a CO-Releasing Molecule with an Extensive Aqueous Solution Chemistry. *Dalton Trans.* **2007**, *15*, 1500−1508.

(6) Seixas, J. D.; Santos, M. F. A.; Mukhopadhyay, A.; Coelho, A. C.; Reis, P. M.; Veiros, L. F.; Marques, A. R.; Penacho, N.; Gonçalves, A. M. L.; Romão, M. J.; Bernardes, G. J. L.; Santos-Silva, T.; Romão, C. C. A Contribution to the Rational Design of Ru(CO) 3 Cl 2 L Complexes for in Vivo Delivery of CO. *Dalton Trans.* **2015**, *44*, 5058−5075.

(7) Desmard, M.; Davidge, K. S.; Bouvet, O.; Morin, D.; Roux, D.; Foresti, R.; Ricard, J. D.; Denamur, E.; Poole, R. K.; Montravers, P.; Morterlini, R.; Boczkowski, J. A Carbon Monoxide-releasing Molecule (CORM-3) Exerts Bactericidal Activity against Pseudomonas Aeruginosa and Improves Survival in an Animal Model of Bacteraemia. *FASEB J.* **2009**, *23*, 1023−1031.

(8) Tavares, A. F.; Parente, M. R.; Justino, M. C.; Oleastro, M.; Nobre, L. S.; Saraiva, L. M. The Bactericidal Activity of Carbon Monoxide-Releasing Molecules against Helicobacter Pylori. *PLoS One* **2013**, *8*, No. e83157.

(9) Murray, T. S.; Okegbe, C.; Gao, Y.; Kazmierczak, B. I.; Motterlini, R.; Dietrich, L. E. P.; Bruscia, E. M. The Carbon Monoxide Releasing Molecule CORM-2 Attenuates Pseudomonas Aeruginosa Biofilm Formation. *PLoS One* **2012**, *7*, No. e35499.

(10) Nagel, C.; McLean, S.; Poole, R. K.; Braunschweig, H.; Kramer, T.; Schatzschneider, U. Introducing [Mn(CO)3(Tpa-K3N)]+ as a Novel Photoactivatable CO-Releasing Molecule with Well-Defined ICORM Intermediates − Synthesis, Spectroscopy, and Antibacterial Activity. *Dalton Trans.* **2014**, *43*, 9986−9997.

(11) Tinajero-Trejo, M.; Rana, N.; Nagel, C.; Jesse, H. E.; Smith, T. W.; Wareham, L. K.; Hippler, M.; Schatzschneider, U.; Poole, R. K. Antimicrobial Activity of the Manganese Photoactivated Carbon Monoxide-Releasing Molecule [Mn(CO)3(Tpa-K3N)]+ Against a Pathogenic Escherichia Coli That Causes Urinary Infections. *Antioxidants Redox Signal.* **2016**, *24*, 765−780.

(12) Betts, J.; Nagel, C.; Schatzschneider, U.; Poole, R.; Ragione, M. L. Antimicrobial Activity of Carbon Monoxide- Releasing Molecule [Mn $(CO)_3$(Tpa- κ3 N)] Br versus Multidrug-Resistant Isolates of Avian Pathogenic Escherichia Coli and Its Synergy with Colistin. *PLoS One* **2017**, *12*, No. e0186359.

(13) Patra, M.; Wenzel, M.; Prochnow, P.; Pierroz, V.; Gasser, G.; Bandow, J. E.; Metzler-Nolte, N. An Organometallic Structure-Activity Relationship Study Reveals the Essential Role of a Re(CO)3 moiety in the Activity against Gram-Positive Pathogens Including MRSA. *Chem. Sci.* **2015**, *6*, 214−224.

(14) Wenzel, M.; Patra, M.; Senges, C. H. R.; Ott, I.; Stepanek, J. J.; Pinto, A.; Prochnow, P.; Vuong, C.; Langklotz, S.; Metzler-Nolte, N.; Bandow, J. E. Analysis of the Mechanism of Action of Potent Antibacterial Hetero-Tri-Organometallic Compounds: A Structurally New Class of Antibiotics. *ACS Chem. Biol.* **2013**, *8*, 1442−1450.

(15) Frei, A.; Zuegg, J.; Elliott, A. G.; Baker, M.; Braese, S.; Brown, C.; Chen, F.; Dowson, C.; Jung, N.; King, A. P.; Mansour, A. M.; Massi, M.; Moat, J.; Mohamed, H. A.; Renfrew, A. K.; Rutledge, P. J.; Sadler, P. J.; Todd, M. H.; Willans, C. E.; Wilson, J. J.; Cooper, M. A.; Blaskovich, M. A. T.; Blaskovich, M. A. T. Metal Complexes as a Promising Source for New Antibiotics. *Chem. Sci.* **2020**, *11*, 2627−2639.

(16) Simpson, P. V.; Nagel, C.; Bruhn, H.; Schatzschneider, U. Antibacterial and Antiparasitic Activity of Manganese(I) Tricarbonyl Complexes with Ketoconazole, Miconazole, and Clotrimazole Ligands. *Organometallics* **2015**, *34*, 3809−3815.

(17) Hubick, S.; Jayaraman, A.; McKeen, A.; Reid, S.; Alcorn, J.; Stavrinides, J.; Sterenberg, B. T. A Potent Synthetic Inorganic Antibiotic with Activity against Drug-Resistant Pathogens. *Sci. Rep.* **2017**, *7*, 41999−42006.

(18) Siegmund, D.; Lorenz, N.; Gothe, Y.; Spies, C.; Geissler, B.; Prochnow, P.; Nuernberger, P.; Bandow, J. E.; Metzler-Nolte, N. Benzannulated Re(i)-NHC Complexes: Synthesis, Photophysical Properties and Antimicrobial Activity. *Dalton Trans.* **2017**, *46*, 15269−15279.

(19) Sovari, S. N.; Radakovic, N.; Roch, P.; Crochet, A.; Pavic, A.; Zobi, F. Combatting AMR.: A Molecular Approach to the Discovery of Potent and Non-Toxic Rhenium Complexes Active against C. Albicans-MRSA Co-Infection. *Eur. J. Med. Chem.* **2021**, *226*, 113858.

(20) Sovari, S. N.; Vojnovic, S.; Bogojevic, S. S.; Crochet, A.; Pavic, A.; Nikodinovic-Runic, J.; Zobi, F. Design, Synthesis and in Vivo Evaluation of 3-Arylcoumarin Derivatives of Rhenium(I) Tricarbonyl Complexes as Potent Antibacterial Agents against Methicillin-Resistant Staphylococcus Aureus (MRSA). *Eur. J. Med. Chem.* **2020**, *205*, 112533−112549.

(21) Moya, S. A.; Guerrero, J.; Pastene, R.; Azócar-Guzmán, I.; Pardey, A. J. Metal Carbonyl Complexes Containing Heterocyclic Nitrogen Ligands Part IX. MnBr(CO)3(3,3′-R-2,2′-Biquinoline) Compounds. *Polyhedron* **2002**, *21*, 439−444.

(22) Franco, F.; Pinto, M. F.; Royo, B.; Lloret-Fillol, J. A Highly Active N-Heterocyclic Carbene Manganese(I) Complex for Selective Electrocatalytic CO_2 Reduction to CO. *Angew. Chem., Int. Ed.* **2018**, *130*, 4693−4696.

(23) Chaves-Ferreira, M.; Albuquerque, I. S.; Matak-Vinkovic, D.; Coelho, A. C.; Carvalho, S. M.; Saraiva, L. M.; Romão, C. C.; Bernardes, G. J. L. Spontaneous CO Release from Ru II (CO) 2 -Protein Complexes in Aqueous Solution, Cells, and Mice. *Angew. Chem., Int. Ed.* **2015**, *54*, 1172−1175.

(24) Seixas, J. D.; Mukhopadhyay, A.; Santos-Silva, T.; Otterbein, L. E.; Gallo, D. J.; Rodrigues, S. S.; Guerreiro, B. H.; Gonçalves, A. M. L.; Penacho, N.; Marques, A. R.; Coelho, A. C.; Reis, P. M.; Romão,

https://doi.org/10.1021/acsbiomedchemau.2c00007
ACS Bio Med Chem Au 2022, 2, 419−436

M. J.; Romão, C. C. Characterization of a Versatile Organometallic Pro-Drug (CORM) for Experimental CO Based Therapeutics. *Dalton Trans.* **2013**, *42*, 5985−5998.
(25) Tavares, A. F. N.; Teixeira, M.; Romão, C. C.; Seixas, J. D.; Nobre, L. S.; Saraiva, L. M. Reactive Oxygen Species Mediate Bactericidal Killing Elicited by Carbon Monoxide-Releasing Molecules. *J. Biol. Chem.* **2011**, *286*, 26708−26717.
(26) Mede, R.; Gläser, S.; Suchland, B.; Schowtka, B.; Mandel, M.; Görls, H.; Krieck, S.; Schiller, A.; Westerhausen, M. Manganese(I)-Based CORMs with 5-Substituted 3-(2-Pyridyl)Pyrazole Ligands. *Inorganics* **2017**, *5*, 8−21.
(27) Michel, B. W.; Lippert, A. R.; Chang, C. J. A Reaction-Based Fluorescent Probe for Selective Imaging of Carbon Monoxide in Living Cells Using a Palladium-Mediated Carbonylation. *J. Am. Chem. Soc.* **2012**, *134*, 15668−15671.
(28) Rice, L. B. Federal Funding for the Study of Antimicrobial Resistance in Nosocomial Pathogens: No ESKAPE. *J. Infect. Dis.* **2008**, *197*, 1079−1081.
(29) Urban, A.; Eckermann, S.; Fast, B.; Metzger, S.; Gehling, M.; Ziegelbauer, K.; Rübsamen-Waigmann, H.; Freiberg, C. Novel Whole-Cell Antibiotic Biosensors for Compound Discovery. *Appl. Environ. Microbiol.* **2007**, *73*, 6436−6443.
(30) Wex, K. W.; Saur, J. S.; Handel, F.; Ortlieb, N.; Mokeev, V.; Kulik, A.; Niedermeyer, T. H. J.; Mast, Y.; Grond, S.; Berscheid, A.; Brötz-Oesterhelt, H. Bioreporters for Direct Mode of Action-Informed Screening of Antibiotic Producer Strains. *Cell Chem. Biol.* **2021**, *28*, 1242−1252.
(31) Schneider, T.; Kruse, T.; Wimmer, R.; Wiedemann, I.; Sass, V.; Pag, U.; Jansen, A.; Nielsen, A. K.; Mygind, P. H.; Raventós, D. S.; Neve, S.; Ravn, B.; Bonvin, A. M. J. J.; De Maria, L.; Andersen, A. S.; Gammelgaard, L. K.; Sahl, H.-G.; Kristensen, H.-H. Plectasin, a Fungal Defensin, Targets the Bacterial Cell Wall Precursor Lipid II. *Science* **2010**, *328*, 1168−1172.
(32) Kuru, E.; Radkov, A.; Meng, X.; Egan, A.; Alvarez, L.; Dowson, A.; Booher, G.; Breukink, E.; Roper, D. I.; Cava, F.; Vollmer, W.; Brun, Y.; VanNieuwenhze, M. S. Mechanisms of Incorporation for D-Amino Acid Probes That Target Peptidoglycan Biosynthesis. *ACS Chem. Biol.* **2019**, *14*, 2745−2756.
(33) Egan, A. J. F.; Errington, J.; Vollmer, W. Regulation of Peptidoglycan Synthesis and Remodelling. *Nat. Rev. Microbiol.* **2020**, *18*, 446−460.
(34) Mascher, T.; Zimmer, S. L.; Smith, T.-A.; Helmann, J. D. Antibiotic-Inducible Promoter Regulated by the Cell Envelope Stress-Sensing Two-Component System LiaRS of Bacillus Subtilis. *Antimicrob. Agents Chemother.* **2004**, *48*, 2888−2896.
(35) Wright, M. A.; Wright, J. A. PhotoCORMs: CO Release Moves into the Visible. *Dalton Trans.* **2016**, *45*, 6801−6811.
(36) Ward, J. S.; Morgan, R.; Lynam, J. M.; Fairlamb, I. J. S.; Moir, J. W. B. Toxicity of Tryptophan Manganese(i) Carbonyl (TryptoCORM), against Neisseria Gonorrhoeae. *Medchemcomm* **2017**, *8*, 346−352.
(37) Ward, J. S.; Lynam, J. M.; Moir, J.; Fairlamb, I. J. S. Visible-Light-Induced CO Release from a Therapeutically Viable Tryptophan-Derived Manganese(I) Carbonyl (TryptoCORM) Exhibiting Potent Inhibition againstE. coli. *Chem.—Eur. J.* **2014**, *20*, 15061−15068.
(38) Albada, B.; Metzler-Nolte, N. Highly Potent Antibacterial Organometallic Peptide Conjugates. *Acc. Chem. Res.* **2017**, *50*, 2510−2518.
(39) Vaara, M. Agents That Increase the Permeability of the Outer Membrane. *Microbiol. Rev.* **1992**, *56*, 395−411.
(40) Davidge, K. S.; Sanguinetti, G.; Yee, C. H.; Cox, A. G.; McLeod, C. W.; Monk, C. E.; Mann, B. E.; Motterlini, R.; Poole, R. K. Carbon Monoxide-Releasing Antibacterial Molecules Target Respiration and Global Transcriptional Regulators. *J. Biol. Chem.* **2009**, *284*, 4516−4524.
(41) Smith, H.; Mann, B. E.; Motterlini, R.; Poole, R. K. The Carbon Monoxide-Releasing Molecule, Corm-3 (Ru(Co) 3cl(Glycinate)), Targets Respiration and Oxidases in Campylobacter Jejuni, Generating Hydrogen Peroxide. *IUBMB Life* **2011**, *63*, 363−371.
(42) Arnett, C. H.; Chalkley, M. J.; Agapie, T. A Thermodynamic Model for Redox-Dependent Binding of Carbon Monoxide at Site-Differentiated, High Spin Iron Clusters. *J. Am. Chem. Soc.* **2018**, *140*, 5569−5578.
(43) Stripp, S.; Sanganas, O.; Happe, T.; Haumann, M. The Structure of the Active Site H-Cluster of [FeFe] Hydrogenase from the Green Alga Chlamydomonas Reinhardtii Studied by X-Ray Absorption Spectroscopy. *Biochemistry* **2009**, *48*, 5042−5049.
(44) Scott, A. D.; Pelmenschikov, V.; Guo, Y.; Yan, L.; Wang, H.; George, S. J.; Dapper, C. H.; Newton, W. E.; Yoda, Y.; Tanaka, Y.; Cramer, S. P. Structural Characterization of CO-Inhibited Mo-Nitrogenase by Combined Application of Nuclear Resonance Vibrational Spectroscopy, Extended X-Ray Absorption Fine Structure, and Density Functional Theory: New Insights into the Effects of CO Binding and The. *J. Am. Chem. Soc.* **2014**, *136*, 15942−15954.
(45) Crowley, P. D.; Gallagher, H. C. Clotrimazole as a Pharmaceutical: Past, Present and Future. *J. Appl. Microbiol.* **2014**, *117*, 611−617.
(46) Yamaguchi, H. Antagonistic Action of Lipid Components of Membranes from Candida Albicans and Various Other Lipids on Two Imidazole Antimycotics, Clotrimazole and Miconazole. *Antimicrob. Agents Chemother.* **1977**, *12*, 16−25.
(47) Bourrez, M.; Molton, F.; Chardon-Noblat, S.; Deronzier, A. [Mn(Bipyridyl)(CO)3Br]: An Abundant Metal Carbonyl Complex as Efficient Electrocatalyst for CO_2 Reduction. *Angew. Chem., Int. Ed.* **2011**, *50*, 9903−9906.
(48) Michels, G. D.; Svec, H. J. Characterization of MnTc(CO)Lo and TcRe(CO)Lo. *Inorg. Chem.* **1981**, *20*, 3445−3447.
(49) Hieber, W.; Fuchs, H. Über Metallcarbonyle. XXXIX. Aminsubstituierte Rheniumcarbonyle. *Z. Anorg. Allg. Chem.* **1941**, *248*, 269−275.
(50) Liu, T.; Wang, L.; Wu, K.; Yu, Z. Manganese-Catalyzed β-Alkylation of Secondary Alcohols with Primary Alcohols under Phosphine-Free Conditions. *ACS Catal.* **2018**, *8*, 7201−7207.
(51) Agarwal, J.; Shaw, T. W.; Stanton, C. J.; Majetich, G. F.; Bocarsly, A. B.; Schaefer, H. F. NHC-Containing Manganese(I) Electrocatalysts for the Two-Electron Reduction of CO_2. *Angew. Chem., Int. Ed.* **2014**, *53*, 5152−5155.
(52) Riera, V.; Gimeno, J.; Laguna, M.; Gamasa, M. P. Synthesis of cationic pentacarbonyl, fac- and mer-tricarbonyl, and cis-and trans-dicarbonyl complexes of manganese(I). *J. Chem. Soc., Dalton Trans.* **1979**, 996−1002.
(53) Chen, J.; Frediansyah, A.; Männle, D.; Straetener, J.; Brötz-Oesterhelt, H.; Ziemert, N.; Kaysser, L.; Gross, H. New Nocobactin Derivatives with Antimuscarinic Activity, Terpenibactins A−C, Revealed by Genome Mining of Nocardia Terpenica IFM0406. *ChemBioChem* **2020**, *21*, 2205−2213.
(54) Nobre, L. S.; Jeremias, H.; Romão, C. C.; Saraiva, L. M. Examining the Antimicrobial Activity and Toxicity to Animal Cells of Different Types of CO-Releasing Molecules. *Dalton Trans.* **2016**, *45*, 1455−1466.
(55) Wenzel, M.; Chiriac, A. I.; Otto, A.; Zweytick, D.; May, C.; Schumacher, C.; Gust, R.; Albada, H. B.; Penkova, M.; Krämer, U.; Erdmann, R.; Metzler-Nolte, N.; Straus, S. K.; Bremer, E.; Becher, D.; Brötz-Oesterhelt, H.; Sahl, H. G.; Bandow, J. E. Small Cationic Antimicrobial Peptides Delocalize Peripheral Membrane Proteins. *Proc. Natl. Acad. Sci. U.S.A.* **2014**, *111*, No. E1409.
(56) Radeck, J.; Gebhard, S.; Orchard, P. S.; Kirchner, M.; Bauer, S.; Mascher, T.; Fritz, G. Anatomy of the Bacitracin Resistance Network in Bacillus Subtilis. *Mol. Microbiol.* **2016**, *100*, 607−620.
(57) Tan, S.; Ludwig, K. C.; Müller, A.; Schneider, T.; Nodwell, J. R. The Lasso Peptide Siamycin-I Targets Lipid II at the Gram-Positive Cell Surface. *ACS Chem. Biol.* **2019**, *14*, 966−974.
(58) Mayer, C.; Sass, P.; Brötz-Oesterhelt, H. Consequences of Dosing and Timing on the Antibacterial Effects of ADEP Antibiotics. *Int. J. Med. Microbiol.* **2019**, *309*, 151329−151332.

https://doi.org/10.1021/acsbiomedchemau.2c00007
ACS Bio Med Chem Au 2022, 2, 419−436

(59) Kuru, E.; Tekkam, S.; Hall, E.; Brun, Y. V.; Van Nieuwenhze, M. S. Synthesis of Fluorescent D-Amino Acids and Their Use for Probing Peptidoglycan Synthesis and Bacterial Growth in Situ. *Nat. Protoc.* **2015**, *10*, 33−52.
(60) Schindelin, J.; Arganda-Carreras, I.; Frise, E.; Kaynig, V.; Longair, M.; Pietzsch, T.; Preibisch, S.; Rueden, C.; Saalfeld, S.; Schmid, B.; Tinevez, J.-Y.; White, D. J.; Hartenstein, V.; Eliceiri, K.; Tomancak, P.; Cardona, A. Fiji: An Open-Source Platform for Biological-Image Analysis. *Nat. Methods* **2012**, *9*, 676−682.
(61) Ducret, A.; Quardokus, E. M.; Brun, Y. V. MicrobeJ, a Tool for High Throughput Bacterial Cell Detection and Quantitative Analysis. *Nat. Microbiol.* **2016**, *1*, 16077−16091.
(62) Saising, J.; Nguyen, M.-T.; Härtner, T.; Ebner, P.; Al Mamun Bhuyan, A.; Berscheid, A.; Muehlenkamp, M.; Schäkermann, S.; Kumari, N.; Maier, M. E.; Voravuthikunchai, S. P.; Bandow, J.; Lang, F.; Brötz-Oesterhelt, H.; Götz, F. Rhodomyrtone (Rom) Is a Membrane-Active Compound. *Biochim. Biophys. Acta, Biomembr.* **2018**, *1860*, 1114−1124.
(63) Kluj, R. M.; Ebner, P.; Adamek, M.; Ziemert, N.; Mayer, C.; Borisova, M. Recovery of the Peptidoglycan Turnover Product Released by the Autolysin Atl in Staphylococcus Aureus Involves the Phosphotransferase System Transporter MurP and the Novel 6-Phospho-N-Acetylmuramidase MupG. *Front. Microbiol.* **2018**, *9*, 2725−2739.
(64) Gisin, J.; Schneider, A.; Nägele, B.; Borisova, M.; Mayer, C. A Cell Wall Recycling Shortcut That Bypasses Peptidoglycan de Novo Biosynthesis. *Nat. Chem. Biol.* **2013**, *9*, 491−493.
(65) Schneider, T.; Senn, M. M.; Berger-Bächi, B.; Tossi, A.; Sahl, H.-G.; Wiedemann, I. In Vitro Assembly of a Complete, Pentaglycine Interpeptide Bridge Containing Cell Wall Precursor (Lipid II-Gly5) of Staphylococcus Aureus. *Mol. Microbiol.* **2004**, *53*, 675−685.
(66) Rouser, G.; Fleischer, S.; Yamamoto, A. Two Dimensional Thin Layer Chromatographic Separation of Polar Lipids and Determination of Phospholipids by Phosphorus Analysis of Spots. *Lipids* **1970**, *5*, 494−496.
(67) Kohlrausch, U.; Höltje, J. V. Analysis of Murein and Murein Precursors during Antibiotic-Induced Lysis of Escherichia Coli. *J. Bacteriol.* **1991**, *173*, 3425−3431.
(68) Umbreit, J. N.; Strominger, J. L. Isolation of the Lipid Intermediate in Peptidoglycan Biosynthesis from Escherichia coli. *J. Bacteriol.* **1972**, *112*, 1306−1309.
(69) Brötz, H.; Bierbaum, G.; Leopold, K.; Reynolds, P. E.; Sahl, H. G. The Lantibiotic Mersacidin Inhibits Peptidoglycan Synthesis by Targeting Lipid II. *Antimicrob. Agents Chemother.* **1998**, *42*, 154.
(70) Schneider, T.; Gries, K.; Josten, M.; Wiedemann, I.; Pelzer, S.; Labischinski, H.; Sahl, H.-G. The Lipopeptide Antibiotic Friulimicin B Inhibits Cell Wall Biosynthesis through Complex Formation with Bactoprenol Phosphate. *Antimicrob. Agents Chemother.* **2009**, *53*, 1610−1618.

https://doi.org/10.1021/acsbiomedchemau.2c00007
ACS Bio Med Chem Au 2022, 2, 419−436